Nuno Rodrigo Cândido Lima

Licenciatura em Engenharia de Micro e Nanotecnologias

Development of functional fibers for wearable applications

Dissertação para obtenção do Grau de Mestre em

Engenharia de Micro e Nanotecnologias

Orientador: Ana Catarina Bernardino Baptista, Pos-doc Researcher, DCM FCT-UNL

Co-orientador: Bruno Miguel Morais Faustino, Pos-doc Reseacher, DCM FCT-UNL

Presidente: Prof. Doutor Hugo Manuel Brito Águas

Arguente(s): Prof. Doutor Rui Alberto Garção Barreira do Nascimento Igreja

Vogal(ais): Doutora Ana Catarina Bernardino Baptista

FACULDADE DE CIÊNCIAS E TECNOLOGIA
UNIVERSIDADE NOVA DE LISBOA

Outubro 2018

Acknowledgments/Agradecimentos

Começo por agradecer Professora Dra. Isabel Ferreira por disponibilizar os diferentes laboratórios e equipamentos que tornou esta dissertação possível. Muito obrigado pela confiança que depositou em mim, e por todas as motivações e ideias que me ofereceu quando eu precisava.

Agradeço também à minha orientadora, Dra. Ana Baptista, por ter paciência e disponibilidade para as minhas dúvidas. Obrigado por ter-me ajudado a evoluir, questionado os meus métodos, oferecendo sempre soluções. E claro pelo trabalho espetacular que fez ao corrigir as minhas primeiras versões desta dissertação

Ao meu co-orientador, Dr. Bruno Miguel Faustino, agradeço por parar o que estava a fazer para me auxiliar sempre que eu necessitava. E claro, por preencher as minhas tardes no GAMRY com canções do Quim Barreiros e muita gargalhada.

Quanto à disponibilização, agradeço a todos os membros da equipa

Almeida, obrigado por me ensinares a mexer no programa de desenho 3D e por teres-me ajudado quando necessitava de ferramentas ou de pequenos remendos. As tuas playlists tornaram aquele pequeno laboratório num local bastante agradável.

David, obrigado pelo conhecimento de química que me transmitiste e por me mostrares como manter um laboratório sempre limpo.

Jaime, obrigado por toda a paciência que arranjaste para as várias necessidades que eu tinha. Sempre com resposta na ponta da língua, tu, o Coroa e o Miguel animavam os vários dias no laboratório.

Sofia, muito obrigado por toda a motivação e ajuda. Apoiaste-me desde o início e muitas vezes direcionaste-me no caminho correto. Agradeço todas as conversas, engraçadas e bastante produtivas, que tornaram muitas tardes fantásticas.

Claro que também tenho que agradecer à minha família, mãe, pai e João, que apesar de não parecer ajudaram-me a seguir em frente e não desistir durante o meu percurso académico. Obrigado pelo apoio e paciência que me deram com tanto carinho.

Babi, eu sei que não tenho sido fácil de lidar nestes últimos tempos, e por isso quero agradecer pela calma que tiveste para comigo e pela compreensão das minhas motivações e escolhas.

Também tenho de agradecer aos meus amigos académicos: Chapa, Débora, Fábio., Miguel, Paixão e Rita, muito obrigado pela vossa amizade que me ajudou a fazer o caminho que sigo hoje.

E claro aos meus amigos de infância: Hugo, Maggie, Pardal, Pera, Pio, Tchioleca, Zé e Zório, podem não ter sido muito relevantes na construção deste trabalho, mas sempre me motivaram a ser melhor no que faço.

Sem todas estas pessoas, este trabalho não teria sido possível.

Deixo uma página em branco para todos os que não me lembrei. Obrigado.

This work was partially funded by ERC-CoG-2014, CapTherPV, 647596, by H2020-ICT-2014-1, RIA, TransFlexTeg, 645241 and by FEDER funds through the COMPETE 2020 Program and National Funds through FCT - Portuguese Foundation for Science and Technology under the project UID/CTM/50025/2013.

Abstract

Wearable energy storage systems have been intensely investigated to cope with the increase in energy demand for wearable electronics. With bulky and rigid energy storage devices being non-practical for wearable technology, one-dimensional fibers show great promise in this area due to good flexibility and adaptation to deformation.

The goal of this thesis was to create a cheap supercapacitor (SC) capable of using simulated body fluids (SBF) as the electrolyte in view of potential applications in the field of wearable electronics, e.g. in biomedical monitoring applications.

In this thesis, different materials were tested as electrodes for a one-dimensional (fiber-shaped) flexible supercapacitor (SC) whilst using cellulose acetate (CA) electrospun fibers as the separator; these included: aluminum (Al) wire and copper (Cu) evaporated on the top of CA fibers; Al wire with Cu wire; Al wire with carbon ink deposited on CA fibers; exfoliated graphite wire or carbon fibers bundle (CF) with Al wire; and a CF symmetrical SC. The later revealing a greater electrochemical cycling stability. Hence, in an attempted to further optimize the CF symmetrical SC architecture, the surface of CFs was further functionalized with a ZnO:PVDF composite and polypyrrole (Ppy). CFs functionalized with Ppy showed a specific capacitance three-fold higher than that of carbon fibers symmetrical SC, an energy density of 159.65 mWh kg^{-1} and a power density of 11.49 W kg^{-1}. Furthermore, replacing the SBF with a 0.1 M of KOH it was possible to achieve higher specific capacitances (3.60 F/g vs. 0.23 F/g at 100 mV/s).

KEYWORDS: Wearable electronics; energy storage; supercapacitor; electrospinning; functional fibers

Resumo

Sistemas de armazenamento de energia flexíveis têm sido intensamente investigados para lidar com o aumento da procura de armazenamento de energia para eletrónica vestível. Como os dispositivos de armazenamento de energia convencionais (volumosos e rígidos) não são práticos para este tipo de tecnologia, as fibras unidimensionais mostram uma grande promessa nesta área devido à boa flexibilidade e adaptação à deformação.

O objetivo desta tese focou-se em criar um supercondensador (SC) barato capaz de usar fluidos corporais simulados (SBF) como eletrólito, tendo como intento aplicações potenciais no campo da eletrónica vestível, como por exemplo, em aplicações de monitoramento biomédico. Nesta tese, diferentes materiais foram testados como elétrodos para um supercondensador flexível (SC) unidimensional (em forma de fibra), mantendo um separador de acetato de celulose (CA) entre eles; estes incluíram: fio de alumínio (Al) e cobre (Cu) evaporado no topo das fibras CA; Fio de Al com fio de Cu; fio de Al com tinta de carbono depositada em fibras CA; fio de grafite esfoliado ou feixe de fibras de carbono (CF) com fio Al; e um SC simétrico de CF. O posterior revelou maior estabilidade em ciclagem eletroquímica. Logo, numa tentativa de otimizar ainda mais este SC, as superfícies dos elétrodos foram funcionalizadas com um compósito de ZnO:PVDF e com polipirrol (Ppy). Os elétrodos funcionalizados com Ppy mostraram uma capacitância específica três vezes superior que o SC simétrico, uma densidade de energia de 159,65 mWh kg^{-1} e uma densidade de potência de 11,49 W kg^{-1}. Porém, substituindo o SBF por 0,1 M de KOH, foi possível obter capacitâncias específicas mais altas (3,60 F/g vs. 0,23 F/g a 100 mV/s).

Palavras-chave: Eletrónica vestível; armazenamento de energia; supercondensador; electrospinning; fibras funcionais.

Contents

List of Figures

List of Tables

Abbreviations

Al/C – Aluminum wire with commercially available carbon ink asymmetrical SC

Al/Cu – Aluminum wire with thermally evaporated copper asymmetrical SC

CA – Cellulose acetate

CD – Galvanostatic Charge and Discharge Cycles

CF – Carbon fibers bundle

CF/Al – Carbon fibers bundle with aluminum wire asymmetrical SC

CF/CF – Carbon fibers bundle symmetric SC

CPE – Constant phase capacitor

Cu/Al – Copper wire with aluminum wire asymmetrical SC

CV – Cyclic Voltammetry

DMAc – Dimethylacetamide

DMF – Dimethylformamide

EDLC – Electrical double layer capacitor

EIS – Electrochemical Impedance Spectroscopy

GE – Exfoliated graphite

GE/Al – Exfoliated graphite and PVDF composite with aluminum wire asymmetrical SC

LIB – Lithium ion battery

Ppy – Polypyrrole

Ppy #1 – *In-situ* polymerization of polypyrrole on the CF

Ppy #2 – Dissolved polypyrrole and deposited on the CF

Ppy#1(CF)/CF – Ppy#1 with CF asymmetrical SC

Ppy#2(CF)/CF – Ppy#2 with CF asymmetrical SC

PVD – Physical Vapor Deposition

PVDF – Polyvinylidene fluoride

Rct – Charge transfer resistance

Ru – Uncompensated solution resistance

SBF – Simulated body fluids

SC – Supercapacitor

SEM – Scanning electron microscopy

Wd – Warburg impedance

ZnO:PVDF(CF)/CF – Zinc oxide and PVDF composite around CF with CF asymmetrical SC

Symbols

C – Capacitance

Q – Charge

V – Potential

$\varepsilon 0$ – Vacuum permittivity

ε – Dielectric permittivity in the medium

A – Electrode/separator interfacial area

d – Distance between electrodes

m – Electrode's mass

v – Potential scan rate

ΔV – Potential sweep window

$I_{(V)}$ – Resulting current from the CV curves

I – Applied current from the CD curves

Δt – Discharge time

E – Energy density

P – Power density

Motivation and Objectives

Wearable electronics and respective technologies are currently in great demand. Devices such as smartwatches, phones, rings, monitoring medical devices and other wearables are trending towards thinner, lighter and foldable ones [1]–[3]. Therefore, energy storage system must adapt to these changes by creating a storage system that can maintain its high energy and power density while simultaneously being submitted to mechanical distortions.

To make a cheap device that can quickly store and release enough energy for powering wearables, aside with maintaining their properties while subjected to mechanical forces has shown to be difficult [1][3]. Batteries and supercapacitors with ingenious 1D, 2D and 3D architectures, over a wide range of different materials, have been widely researched in the last few years [1]–[3]. Towards making such a device, flexible electrodes, current collectors and separator must use a safe electrolyte for operating. Most of the existing devices use interesting materials like graphene and specific metal oxides (MnO_2 or ZnO) for the electrodes which are obtained by expensive processes [1][2].

In this thesis, an energy storage device for wearable applications with a 1D configuration, that must be flexible and possess no dangerous materials to the user is attempted. Structurally, a coaxial approach was preferred with the outer electrode painted or twisted around the separator, directly deposited on the inner electrode. Different cheap electrode materials were also tested while consistently maintaining an electrospun cellulose acetate (CA) separator embedded with a simulated body fluid (SBF) solution. This work aims the development of a cheap wearable energy storage device activated by biological fluids without the need of encapsulation envisaging health conditions monitorization.

1. Introduction

1.1. Energy storage systems

In the last decade, wearable energy storage systems have been intensively investigated due to the urgent need for replacing fossil fuels with clean energy. To make sure clean energy is feasible, means of creating a viable energy storage system must be complied. As for wearable applications like smartphones, smartwatches, biomedical devices, functionalized fabric or even smart tattoos (Figure 1.1), the trend of thinner, lighter and flexible components brings difficulties in creating a complying energy storage system. In addition to the previous characteristics, wearable energy storage must have high energy and power density, operationally safe and possess a long stable cycling life to power wearable electronic devices efficiently [1]–[5]. Batteries and supercapacitors (electrical double layer capacitor (EDLC) and pseudocapacitors) are the most researched type of devices [3][4]. In order to achieve such a device different electrode materials and configurations have been investigated [1][3][4].

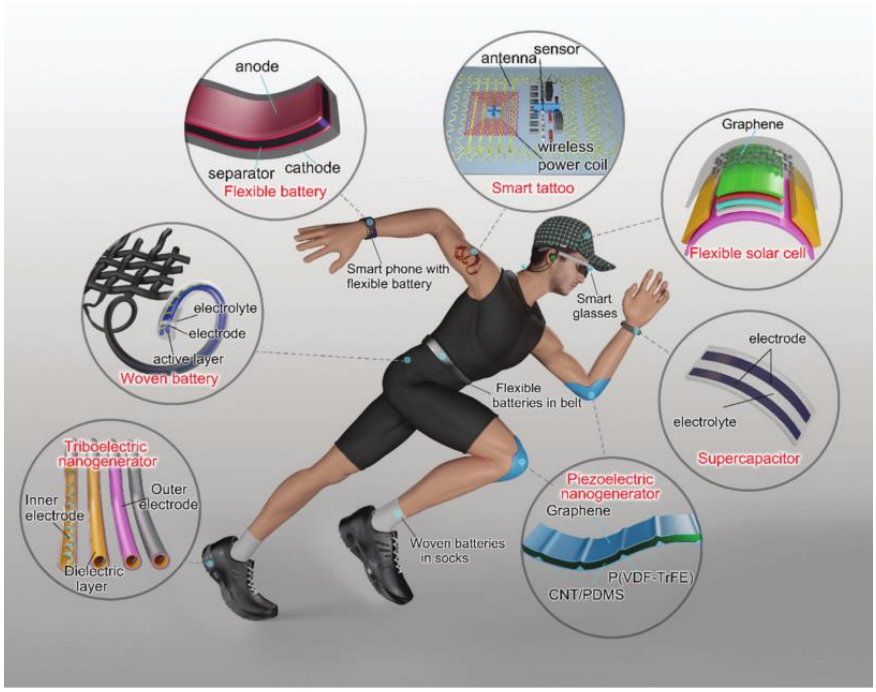

Fig. 1.1. Schematic of a possible near future for wearable electronics. Adapted from [3].

1.1.1. Device's architecture

Various architectures have been studied to overcome the mechanical properties issue [2]. By using different device configurations, such as one-dimensional (1D) fibers, two-dimensional papers and even three-dimensional sponge like structures [1]–[4], [6]–[9] incorporating energy storage in wearable electronics induces a bigger compliance. 1D structures are probably the most adaptable to wearable clothing, with fiber-like structures ranging from tens to hundreds of micrometers, capable of being, woven and adapted to textiles and other deformable structures [1][7]. These structures are usually

coaxial (core-shell) or two different electrode fibers twisted around each other (Figure 1.2). Coaxial fibers have a core-shell architecture with an inner electrode fiber and an outer electrode layer, separated by the ion conductor. However, these outer layers are very thin, thus difficulties have been found trying to make this layer adaptable to the device's mechanical strength and electrical requirements [1].

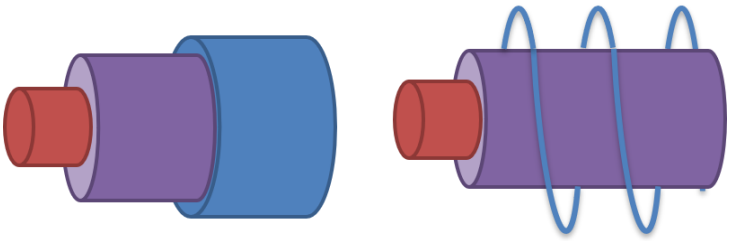

Fig. 1.2. Illustration of the core-shell structure on the left, and the twisted fibers on the right. Where red is the inner electrode, purple is the separator and blue is the outer electrode.

1.1.2. Batteries

Batteries are the most common energy storage system for wearable applications [1][3]. Composed by current collectors and two high capacity electrodes separated by an ionic conductor (usually a non-conductive material filled with electrolyte), batteries store energy by converting electrical energy into chemical energy, and vice-versa [4]. Using this mechanism, they can achieve high energy densities [4]. Specifically, lithium ion batteries (LIB) which are the most common due to their long cyclic life and high energy density [3][6]. However, conventional LIBs do not support flexibility nor the required safety for wearable electronics applications [1][6]. As already mentioned, to overcome this issue coaxial architectures can be considered. Y. Wang *et al.* [6] 3D printed two fiber-like electrodes containing carbon nanotubes and lithium composites, which were twisted around each other separated by a gel electrolyte (Figure 1.3). Using this architecture their best result showed suitable mechanical strength and flexibility accompanied with good capacitance (164.8 mAh g^{-1} at 50 mA g^{-1}) and cycling stability (160 mAh g^{-1} after 30 cycles, with nearly constant 3.37 V) [6].

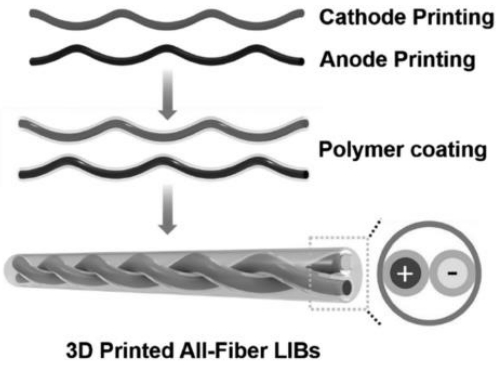

Fig. 1.3. Schematic of the fabrication of 3D-printed fiber LIB. Adapted from [6].

Other elements-based battery materials have been considered in an attempt to replace lithium with cheaper and safer materials, e.g. aluminum (Al) and zinc (Zn) [9]–[11]. Zinc-based electrodes are often a choice due to their good theoretical specific capacitance (820 A h kg^{-1}), non-toxicity and non-flammability. Nevertheless, it only produces about 1.65 V of cell voltage which is considerably lower when compared to lithium (3.6 V) [7]. Aluminum-based batteries are frequently also a choice due to their low cost, increased safety and three-electron redox properties [3][11].

1.1.3. Supercapacitors

Supercapacitors (SC) are a class of capacitors that use two electrodes separated by an ionic conductive medium [3][2]. This class of capacitors presents outstanding capacitance when compared to the conventional capacitors, although the same laws of physics govern their behavior. Therefore, the following equation (1) that is used to describe the capacitance behavior of parallel electrodes can be used to describe the electrode/electrolyte interface in SC as well [12][13].

$$C = \frac{Q}{V} = \frac{\varepsilon 0 * \varepsilon * A}{d} \quad (1)$$

Where *C* is the capacitance in farads (F), *Q* is the accumulated charge in coulombs (C), *V* is the working potential in volts (V), ε is the dielectric permittivity in the medium, ε_0 is the vacuum permittivity ($8.854*10^{-12}$ F/m), *d* is the distance of the Helmholtz layer (between electrodes in conventional capacitors) in meters (m) and *A* is the electrode/separator interfacial area in square meters (m^2) [13]. In SC this equation can only simulate the electrode/electrolyte interface which has very small distance between them (d can be obtained from the radius of the solvate ions), thus achieving very high capacitance [12]. The full device can be modeled as two very low "*d*" capacitors in series. For higher specific capacitances, SC take advantage of their electrode's high specific area as well [2]–[4]. However, for a cylindrical (coaxial) capacitors the resulting capacitance must be described by the following equation (2).

$$C = \frac{Q}{V} = \frac{2\pi * \varepsilon 0 * L}{\ln(\frac{b}{a})} \quad (2)$$

Where *L* is the device's length, *a* is the inner electrode's radius and *b* is the radius from the outer electrode's inner surface.

1.1.3.1. Electrical double layer capacitors

To achieve such high surface area, electrode materials are usually very porous (carbon materials) to enable a superior ion adsorption. Supercapacitors that solely use this storing mechanism are called electrical double layer capacitors (EDLC) due to the adsorption of ions at the interface of the electrodes with the separator, originating two parallel strong electric fields [2][4][13]. Such electrochemical energy storage devices are ideally suitable for fast energy storage and release [2][14]. Since supercapacitors usually store charge using fast ion adsorption/desorption that involve no chemical reactions, high charge/discharge rates or power density are easily achieved [2][3][14]. As an

energy storage and delivery device these rank behind batteries in energy density but compensate with great cycling life and high power density [2][3][15][16]. V. Thong *et al.* [16] reported a coaxial fiber SC with all carbon electrodes (Figure 1.4) with great flexibility, good capacitance (9 F/g at 100 mV/s), cycling stability (retained 88% of initial capacitance after 1000 cycles) and good energy and power density (0.7 µWh/cm and 13.7 µW/cm) [16].

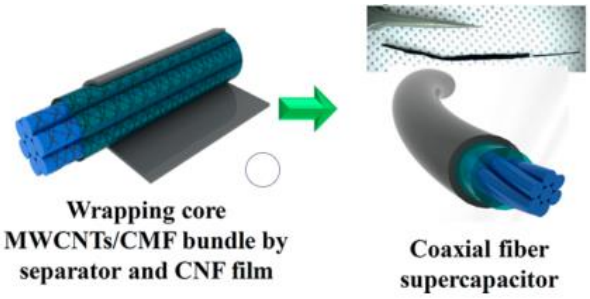

Fig. 1.4. Schematic of the final process of the all carbon SC. Adapted from [16].

1.1.3.2. Pseudocapacitors

Efforts have been made to improve the SCs energy density by using pseudocapacitive materials on the electrode, which use fast redox reactions near the electrodes surface to store charge [2][4]. Metal oxides and conductive polymers, more specifically ZnO, MnO_2 and polypyrrole (Ppy), have been reported to improve the energy density while maintaining or improving their power density [4][16-21]. A. Rafique *et al.* [18] reported a copper wire coated in a ZnO/graphite composite fiber electrode (Figure 1.5). Two of the fibers were later covered with a polymeric electrolyte to serve as separator in a symmetrical SC [18]. The resulting SC showed a very high specific capacitance (27 F/g at 10 mV/s), good flexibility and electrochemical cyclic stability (retained 95% of initial capacitance after 500 cycles)[18].

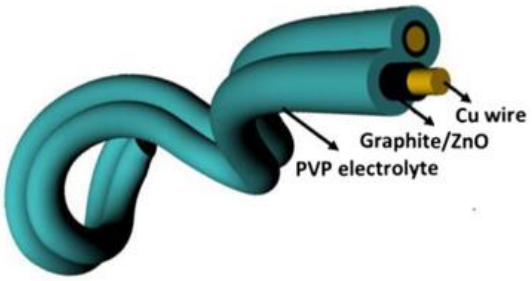

Fig. 1.5. Schematic of A. Rafique et al. parallel electrode fiber SC. Adapted from [18].

Another example is provided by Y. Hu *et al.* [19] which, by using a wet-spinning technique, they achieved graphene/Ppy composite fiber-shaped electrodes (Figure 1.6), and intertwined two of them with a gel electrolyte separating them [19]. Using this technique their SC showed lightweight, optimal flexibility and good, stable capacitance (65-72 F g^{-1}, bended or straight, for 1000 cycles) [19]. This type of SC is called pseudocapacitor and it possesses qualities to make an ideal device for wearable energy

storage. For an optimal device, these could be used while incorporated with an energy harvesting system for sustainable power systems [3].

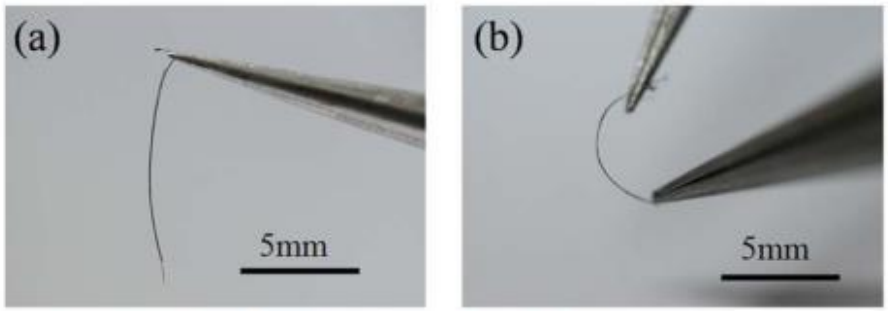

Fig. 1.6. Photo of Y. Hu et al. G/Ppy fiber symmetrical SC free (a) and bended (b). Adapted from [19].

1.2. Electrode materials

The choice of the electrode material defines the type of energy storage mechanism. Normally metallic electrodes tend to have long duration reactions that result in lower power density but high energy density. These electrodes are usually found in batteries and hybrid devices. In SCs, researchers try to find an electrode that can work as current collector, showing great electrical conductivity supported by high porosity/specific area. For a better energy density performance, pseudocapacitve materials like metal oxides or conductive polymers can improve the device's capacitance [1][3][20]. In EDLCs high specific area carbon materials are used, they usually undergo through additional processing in order to increase their porosity and consequently their specific area [7]. To greatly increase the performance of SCs new structures with pseudocapacitive and electrical double layer materials have been created [7][21][22]. However, these structures usually undergo through expensive and complex processing. To avoid heavy expenses, conductive polymers are the prime choice, possessing good electrochemical properties and similar processability to conventional polymers [19][20][23].

In this work electrospun cellulose acetate (CA) fibers served as separator in all samples due to its high surface area and ion permeability [24]. Initially, high purity Al wires served as inner electrode in battery-supercapacitor hybrid configurations with evaporated copper (Cu) or carbon ink as outer electrode. Then a twisted electrodes approach was taken by using Cu wire, exfoliated graphite/ polyvinylidene fluoride (GE/PVDF) composite wire or carbon fiber threads (CF) with the Al wire. In all built devices, a simulated body fluids (SBF) solution was used as the electrolyte due to its ionic similarity to body fluid . This solution contained corroding ions that can break down the passive oxide layer and lead to pit formation on the metallic electrode [11][25]. This problem was not foreseen, consequently the created devices showed very low cycling stability. Therefore, a CF symmetrical SC was built successfully with good electrochemical stability. The electrochemical properties were increased by functionalizing the CF with a ZnO:PVDF composite ink or a Ppy layer.

2. Materials and Methods

2.1. Electrospinning of CA fibers

A 12% wt, CA solution was made by dissolving CA (Sigma-Aldrich®, Mn = 61 000 with 40% acetyl groups) in acetone and dimethylacetamide (DMAc) in a 2:1 (wt) proportion and magnetically agitated. The solution was loaded onto a 1 mL syringe with a 21-gauge needle tip. A 6 x 6 cm frame was designed using Autodesk Fusion 360 software and 3D printed to serve as support for the wire substrates in the electrospinning process (Figure 6.1, Supportive Information). Different materials were used as substrate to collect the electrospun fibers during the electrospinning process (working as the inner electrode), namely aluminum (Al, Alfa®, 250 µm of diameter, purity = 99.999%), copper (Cu, recycled electrical circuit), exfoliated graphite/ polyvinylidene fluoride (PVDF, Alfa Aesar®) composite (GE/PVDF) and carbon fibers bundle (CF, Carbon Tenax®, 218 Ω/m). The process was carried out using previously studied and reported parameters in [24], with the equipment layout shown in Figure 6.2, in Supportive Information. These occurred under controlled environmental conditions with a temperature range of 20-25 ºC and a relative humidity between 35-45 %. Different deposition times were tested, 15, 30 and 60 minutes per side; the respective results are shown on chapter 6.4.

2.2. Electrode materials

Thermally evaporated copper, copper wires and aluminum wires served as metallic electrode and current collector for the prepared devices. The thermally evaporated copper was deposited on to aluminum wires, covered with cellulose acetate, using physical vapor deposition (PVD). The deposition occurred at 4.3×10^{-6} mbar at a rate of 1.2 nm s^{-1} and achieved 550 ± 10 nm of thickness.

A ZnO:PVDF ink was synthetized to serve as a shell electrode or electrode functionalization for some devices. The ZnO:PVDF ink was prepared by dissolving 2.75 g of powdered ZnO (Sigma-Aldrich®, Mw = 81.39 g mol^{-1}, particle size < 100 nm) and 0.75 g of PVDF in 4 ml of n.n-dimethylformamide ($HCON(CH_3)_2$, Carlo Erba Reagents®, DMF, purity = 99.8 %). Magnetic agitation and sonication were used to obtain a homogeneous ink.

A commercially available conductive carbon ink (Bare Conductive®) was used to paint the outer electrode directly on to the cellulose acetate layer making a core-shell structure. Afterwards, exfoliated graphite (GE) wires were synthesized for twisted structures. Like the previously discussed ZnO:PVDF ink, exfoliated graphite powder was dissolved with PVDF in DMF. The made solution was loaded into a 1 ml syringe and extruded continuously in to a tub filled with distilled water to form wire shapes. After the wires dried, they were tested for mechanical strength (manually) and electrical resistance with a multimeter. The best working samples were later covered in CA and wrapped in Al wire (Figure 6.3, Supportive Information). Finally, commercially available CF was used as received for SC electrodes (Figure 6.4, Supportive Information), showing optimal mechanical strength and good electrical conductivity (~ 10 Ω in 2 cm). Further functionalization to improve their performance was achieved by

coating the fibers with the previously synthesized ZnO:PVDF ink or Ppy. A first attempt included a simple polymer dissolution process by dissolving 0.215 mg of Ppy (kindly provided by FEUP) in 3 mL of acetone followed by sonication; another approach was considered using the *in-situ* polymerization of pyrrole (C_4H_5N, Sigma-Aldrich®, Mw = 67.09 g mol^{-1}, purity = 98%) (Figure 6.4, Supportive Information) adapted from an already published procedure [24].

2.3. Morphological characterization

Most samples were subjected to scanning electron microscopy (SEM, Hitachi S2400) to analyze surface morphology. Studied samples were carefully selected due to limited availability of the instrument, these were: the thermally evaporated copper, the Al wire (pre and post-cycling) and the CF.

2.4. Electrical and electrochemical characterization

The electrochemical characterization was carried out by cyclic voltammetry (CV), galvanostatic charge and discharge cycles (CD) and electrochemical impedance spectroscopy (EIS) using a potentiostat Gamry Instruments-Reference 3000. All experiments used a two-electrode setup and SBF as the liquid electrolyte (adapted from [26], composition in Table 6.2, Supportive Information) soaking the CA separator (Figure 6.5, Supportive Information). In order to calculate the specific capacitance (F/g), energy density (E, kW/kg) and power density (P, Wh/kg) from the curves, the following equations were used [13]:

$$\frac{C}{m} = \frac{1}{m * v * \Delta V} * \int I_{(V)} dV \quad (1)$$

$$\frac{C}{m} = \frac{I * \Delta t}{m * \Delta V} \quad (2)$$

$$E = \frac{C * (\Delta V)^2}{2} \quad (3)$$

$$P = \frac{E}{t} = \frac{I * \Delta V}{2} \quad (4)$$

Where $\frac{C}{m}$ is the specific capacitance (eq.1 for CV, eq.2 for CD), m (g) is the electrode's mass, v (mV/s) is the potential scan rate, ΔV (V) is the sweep potential window, $I_{(V)}$ (A) is the resulting current from the CV curves, I is the applied current and Δt (s) is the discharge time. In the CV curves, results were extrapolated from a certain potential interval.

3. Results and Discussion

Different electrode´s materials and device´s configurations using CA electrospun fibers as the separator, soaked with SBF (composition from [26]) were evaluated. Table 3.1 shows all structures and configurations studied in this thesis.

Table. 3.1. Various material configurations used on the built supercapacitors with electrospun CA fibers as separator.

Structure	**Inner electrode**	**Outer electrode**	**Configuration**
A: Al/Cu	Al wire	Cu (PVD)	Core/Shell
B: Al/C	Al wire	Carbon ink	Core/Shell
C: Cu/Al	Cu wire	Al wire	Twisted
D: GE:PVDF/Al	GE:PVDF	Al wire	Twisted
E: CF/Al	CF	Al wire	Twisted
F: CF/CF	CF	CF	Twisted
G: ZnO:PVDF(CF)/CF	CF	ZnO:PVDF(CF)	Twisted
H: Ppy#1(CF)/CF	Ppy#1(CF)	CF	Twisted
I: Ppy#2(CF)/CF	Ppy#2(CF)	CF	Twisted

3.1. Metallic electrodes

Initially Al wire was used as counter electrode due to its higher electronegativity. In core-shell configurations the wires were used as inner electrode for its mechanical robustness and high electrical conductivity. Different working electrode materials were tested, namely copper (wire and thermally evaporated), commercial carbon ink, GE:PVDF composite and CF. However, structures using Al wire as inner electrode showed a poor electrochemical stability in SBF. As an alternative, CFs were used as

the inner electrode and later functionalized with a ZnO:PVDF or Ppy layer to improve its electrochemical performances.

3.1.1. Aluminum core-shell configuration

Figure 3.1 shows cyclic voltammograms obtained with Al wire core-shell configurations. A very poor cycling stability is observed which can possibly be attributed to the breakdown of the passivation layer (called “pitting corrosion”) due to the presence of chloride ions in SBF used as the electrolyte [25]. In both structures, Al/Cu (PVD) and Al/C (ink), the device was subjected to 30 cycles and fresh electrolyte was added every 10 cycles. Figure 3.1 (a) and (b) show that the electrochemical behavior of both structures is clearly affected by cycling measurements.

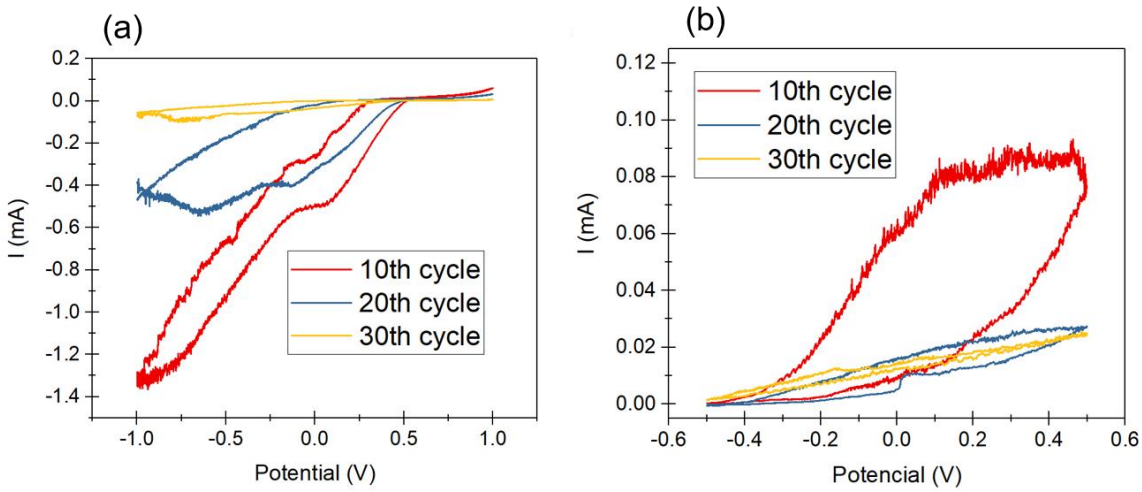

Fig. 3.1. Voltammograms of Al/Cu (PVD) (a), and Al/C (b). Showing the 10th, 20th and 30th cycle.

The structural stability of the electrodes is one of the most relevant factors determining the electrochemical behavior and lifetime of 1D energy harvesting devices. Morphological characterization of inner and outer electrodes was carried out before and after electrochemical cycling measurements to evaluate the uniformity and integrity of the coating.

Figure 3.2 shows the SEM images of the Al wire coated with CA electrospun fibers (cross-section) just before (a) and after (b) electrochemical cycling measurements in SBF. From these images it is observed that the materials crack after electrochemical measurements which strongly affects the device mechanical robustness and explains the loss of electrochemical stability.

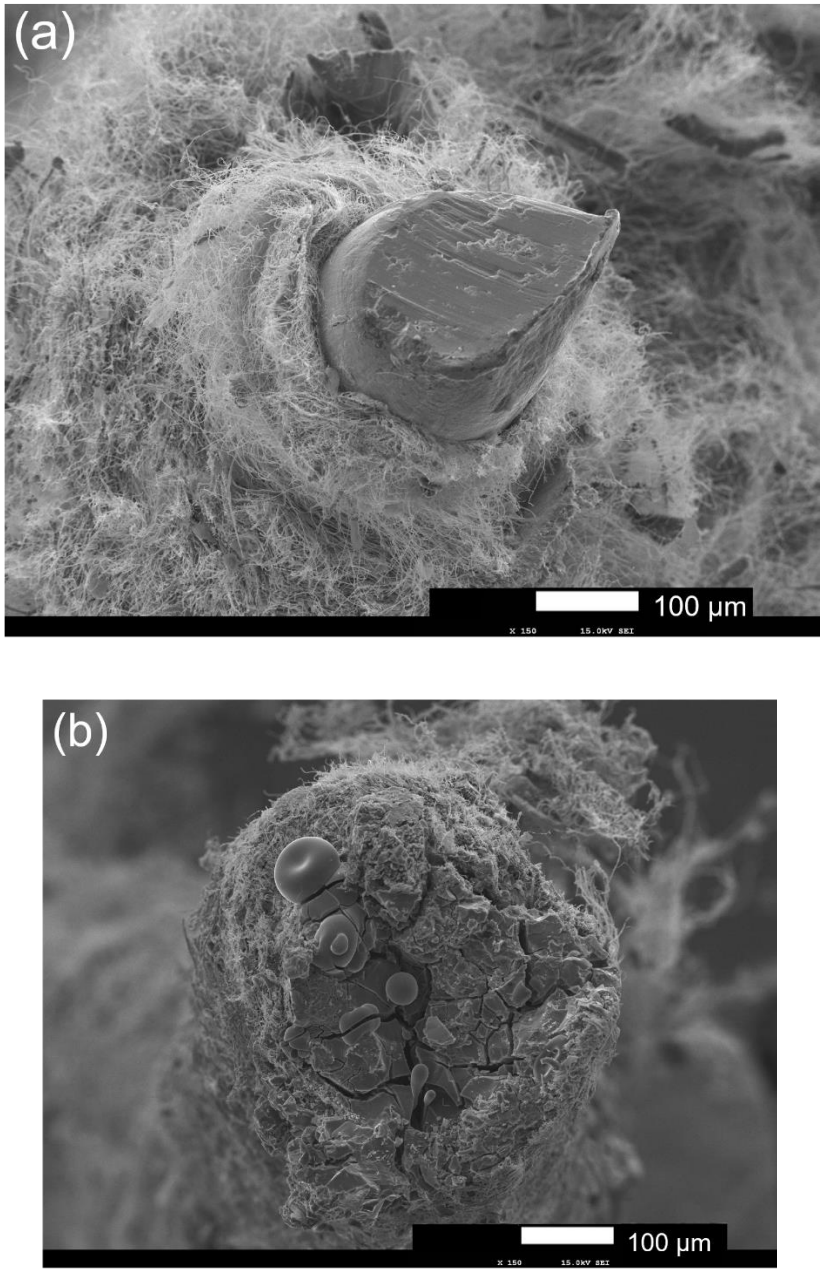

Fig. 3.2. SEM images of Al wire coated with CA fibers (a) before and (b) after electrochemical cycling tests.

Regarding the Al/Cu (PVD) structure, the SEM image of the Cu layer (550 ± 10 nm) deposited by physical vapor deposition (PVD) on CA electrospun fibers (which covers Al wire electrode) is displayed on Figure 3.3. The fibers showed a complete and uniform copper coating, which explains their low electrical resistance (< 10 Ω). However, when the device is subjected to several CV cycles with SBF, the Cu layer started to peel off (due to its weak adhesion) from the fiber´s surface and thus affecting the electrical conductivity and physical integrity of the electrode – as observed in Figure 3.4.

When carbon ink is used (as the outer electrode) to coat the CA fibers, the same phenomenon was verified. After several CV cycles in SBF, the active material showed a poor adhesion to fibers affecting the device´s electrochemical performances and integrity.

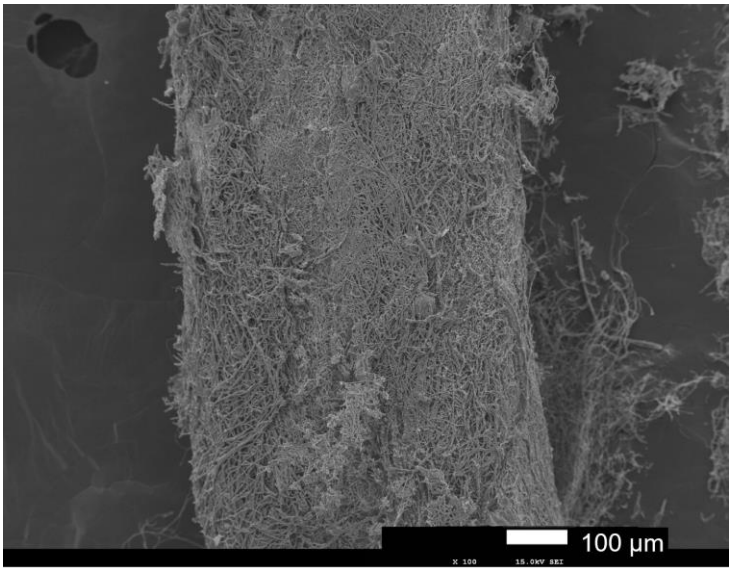

Fig. 3.3. SEM image of thermally evaporated copper coating CA fibers (Al wire as inner electrode).

Fig. 3.4. Photograph of the Al/Cu (PVD) before (a) and after (b) electrochemical cycling tests.

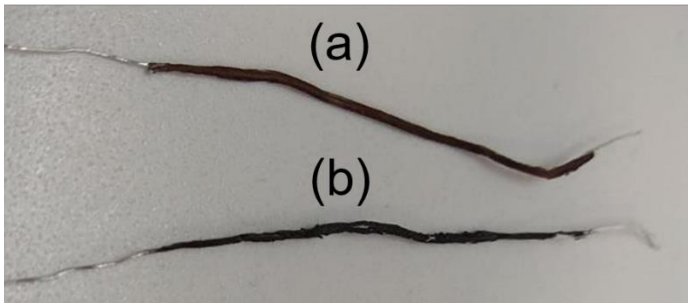

Fig. 3.5. Photography of Al/C, before (a) and after (b) electrochemical cycling tests.

In summary, these two first attempts reveled that either Copper or Carbon ink coatings (as outer electrodes) did not confer structural and electrochemical stability to devices. Both easily cracked and peeled off from CA fiber´s soaked with SBF and loss of electrical conductivity was observed. The outer layer needs to have a greater adhesion to fibers and must conform to the separators surface.

3.1.2. Aluminum twisted configuration

Aluminum wires were then tested as outer electrode, twisted around the separators surface (device with twisted configuration). As inner electrode materials, Cu wire, GE:PVDF composite wire and CF were studied (Figure 3.6).

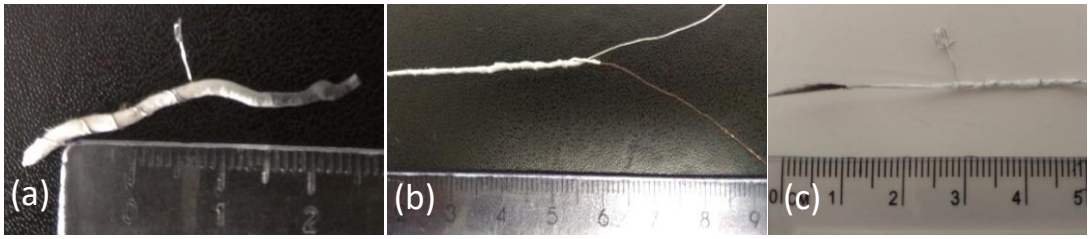

Fig. 3.6. Photography of the made samples with aluminum wires (outer electrode) wrapped around CA covered GE/PVDF(a), a Cu wire (b) and CF (c).

In general, samples shown in Figure 3.6 showed good mechanical robustness. However, the GE:PVDF inner electrode was not tough enough to avoid breaking under deformation and for that reason it was not considered as a good candidate for wearable applications. Nevertheless, the electrochemical characterizations of the above electrodes were carried on.

Figure 3.7 shows the voltammograms obtained for GE:PVDF/Al wire structure at different scan rates. As expected, the device displayed an unstable electrochemical cycling behavior due to the cracking of Al wire and/or GE:PVDF mechanical fragility.

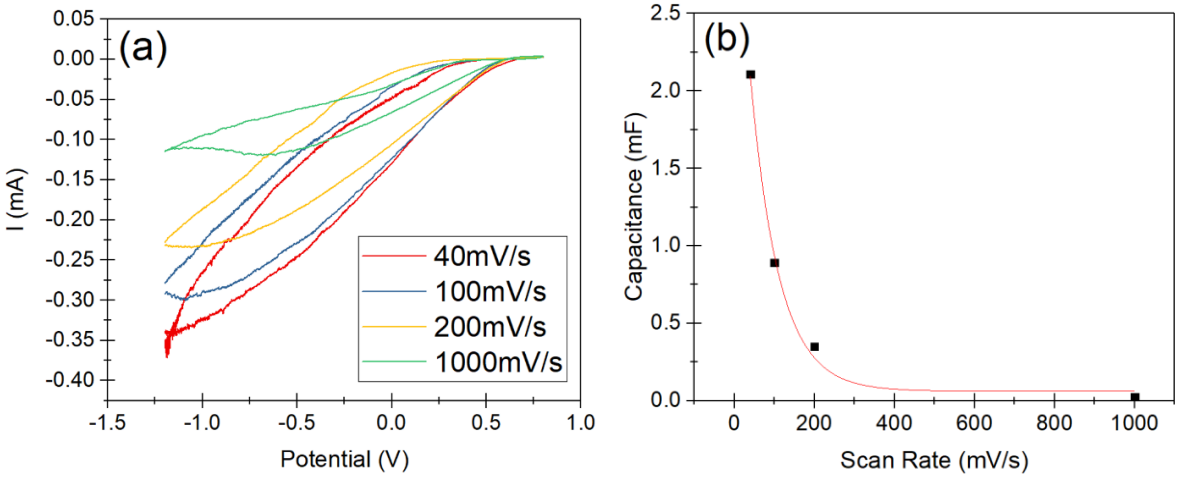

Fig. 3.7. Voltammograms of GE:PVDF/Al. Cycling with different scan rates (a) and the calculated capacitance of each scan rate (b).

Two metallic electrodes in wire form were twisted around each other, Al as counter/reference and Cu as the working electrode. The voltammogram obtained for Cu/Al wire structure is depicted in Figure 3.8. There is a noticeable increase of current values (-1.58 mA at 40 mV/s) and capacitance (6.26 mF at 40 mV/s) when compared with the previous device. This enhancement can be due to the better electrical conductivity of the working electrode. Nevertheless, the capacity decreases

exponentially with increasing scan rates, and the electrochemical cycling stability is not observed (Figure 3.9).

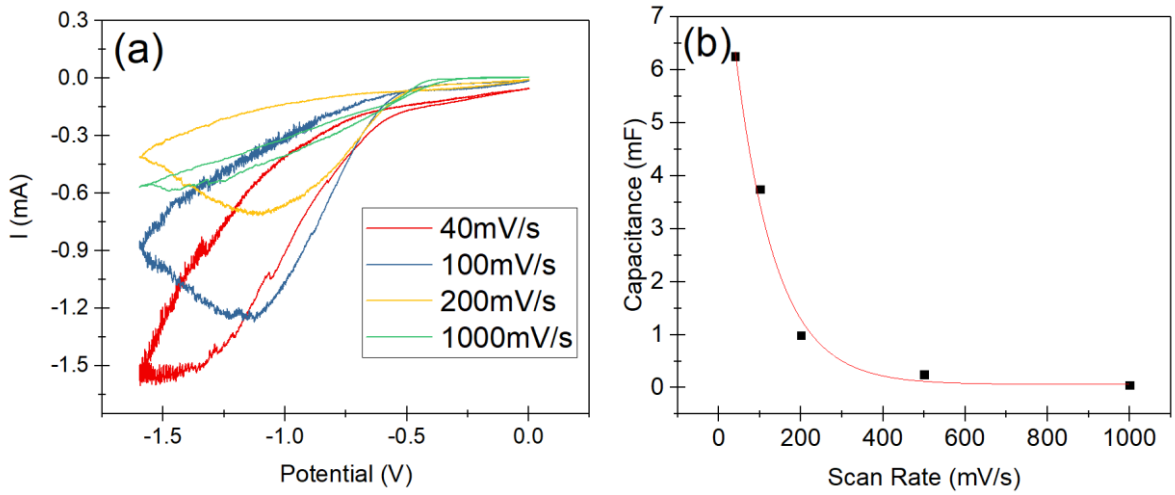

Fig. 3.8. Voltammograms of Cu/Al. Cycling with different scan rates (a) and the calculated capacitance of for each scan rate (b).

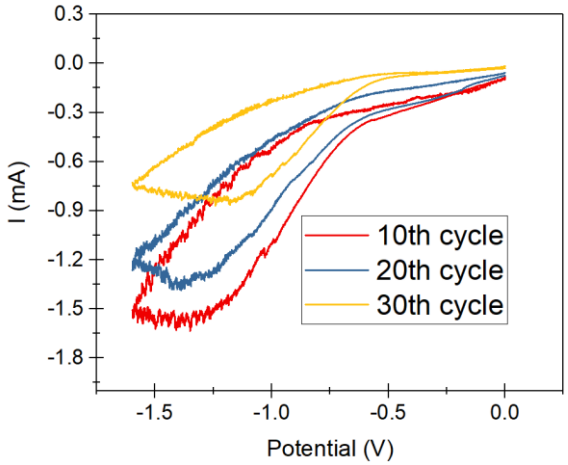

Fig. 3.9. Voltammogram of Cu/Al sample. Showing the 10th, 20th and 30th cycle.

Looking for a flexible and electrochemical stable inner electrode, CF were studied. The commercial carbon fiber thread has high electrical conductivity and can withstand mechanical deformation, making it a candidate for wearable energy storage electrode. Figure 3.10 shows SEM image (cross-section) of CF uniformly coated with CA electrospun fibers.

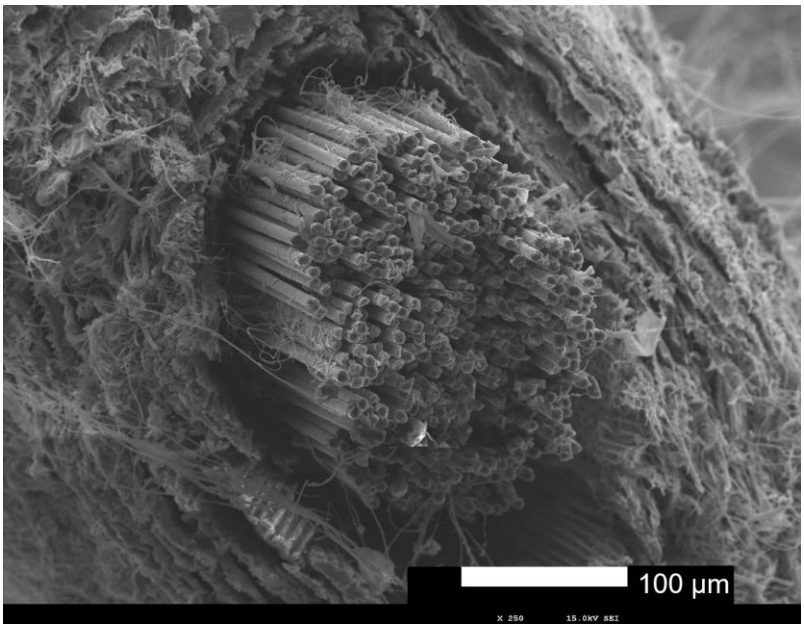

Fig. 3.10. SEM image of the cross-section from CF covered with CA.

An alternative study was considered using an Al wire (as electrode) wrapped around a CF thread coated with CA. Cyclic voltammograms are shown on Figure 3.11 (a); like the precedent, this sample shows an unusual curve but with a maximum current of -0.474 mA at 60 mV/s, which is inferior than that of the Cu/Al wire. Similarly to the previous structures, the capacitance decreases exponentially with increasing scan rates (Figure 3.11 (b)). Unfortunately, the device showed unstable electrochemical cycling (Figure 3.11 (c)), even after re-soaking the CA layer with more SBF the device's properties kept deteriorating with increasing cycling number up until the Al wire broke. This occurrence can possibly be associated to the pitting phenomenon on the Al surface electrode which may contribute to wire structural instability [25].

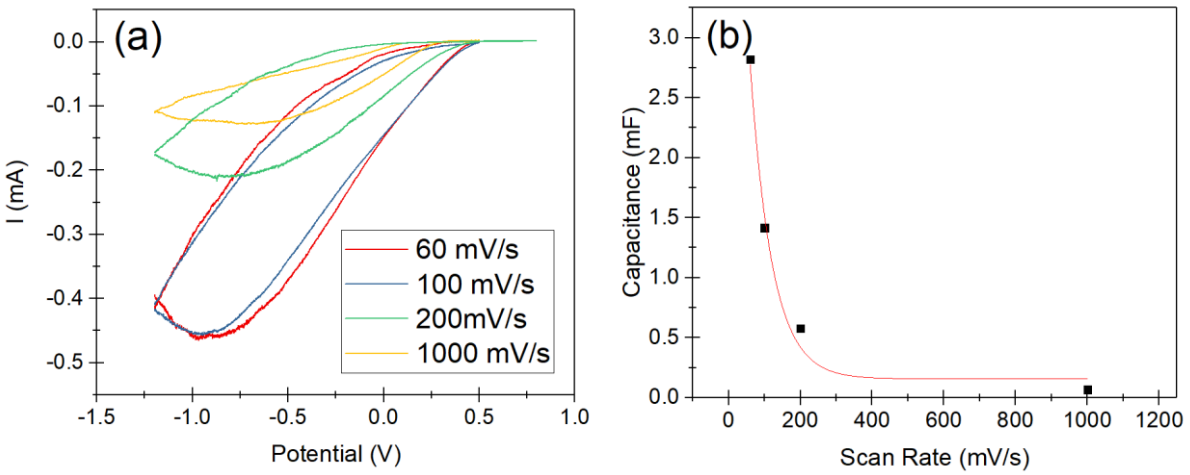

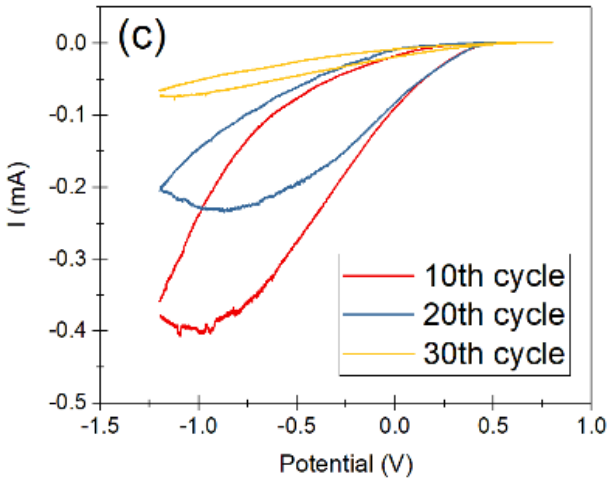

Fig. 3.11. Voltammograms of CF/Al. Cycling with different scan rates (a), the calculated capacitance of each scan rate (b) and the cycling stability (c) showing the 10th, 20th and 30th cycle.

3.2. CF electrodes

Moreover, a CF/CF supercapacitor was also studied (Figure 6.4, Supportive Information). CV curves obtained for the twisted CF symmetrical supercapacitor (Figure 3.12 (a)) show a typical deformed rectangular shape which is characteristic of a capacitor behavior with a maximum current of 51 µA at 100 mV/s. However, due to the deformed shape, it is known that the device possesses a considerable value for its series (electrode and contact resistance) and parallel (ion diffusion) resistance, as expected [13].

The device showed high flexibility, structural robustness and electrochemical cycling stability. However, in Figure 3.12 (b) it is shown a small charge accumulation resulting in low capacitance values, 469.5 µF (62.6 mF/g) at 40 mV/s. While at high scan rates its capacitance is comparable to all of the previous samples (123 µF vs. 62 µF at 1000 mV/s), it was also verified that these cycles are formed in a clockwise direction and increase their electrical current with higher scan rates while the ones that uses Al wires show a counter-clockwise direction and decrease electrical current at higher scan rates. Since the energy storage mechanism found in metals is reaction dependent, time is required to acquire higher capacitance and current values, which could explain the difference.

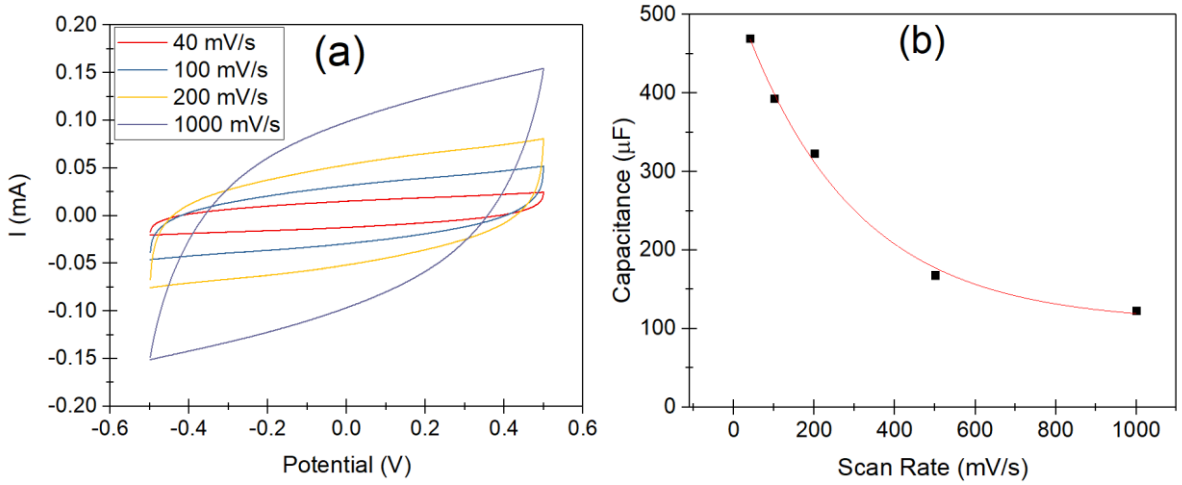

Fig. 3.12. Voltammograms of the CF symmetrical SC. Cycling with different scan rates (a) and the calculated capacitance for each scan rate (b).

To improve the electrochemical performance of the previous structure, the CF thread surface was functionalized with ZnO:PVDF and Ppy. The functionalization of these fibers with highly porous materials can increase the available specific surface area for ion adsorption. In a first approach, ZnO:PVDF ink was used to improve the devices performance. The ZnO:PVDF was drop-casted on to a CF and dried. The resulting electrode was significantly heavier and demonstrated lower flexibility, yet, an improvement was expected. A CA covered CF was then twisted around the ZnO:PVDF(CF) wire.

The CV curves obtained for the ZnO:PVDF(CF)/CF are shown Figure 3.13. As observed, from Figure 3.13 (a) the maximum current at 100 mV/s is 47 µA which is lower than the CF/CF sample (51 µA). Figure 3.13 (b) shows the calculated capacitance for each scan rate on Figure 3.13 (a) and 1000 mV/s. It's noticeable that the capacitance values are lower compared with the CF/CF SC (336 µF vs. 393 µF at 100 mV/s) but displays a higher value at higher scan rates (237 µF vs. 123 µF at 1000 mV/s).

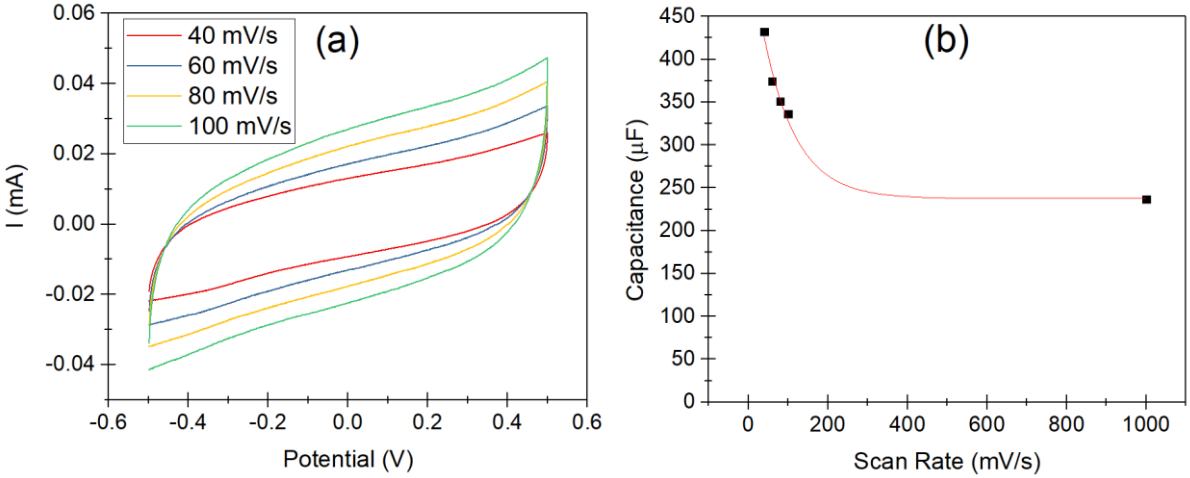

Fig. 3.13. Voltammograms of ZnO:PVDF(CF)/CF. Cycling with different scan rates (a) and the calculated capacitance for each scan rate and 1000 mV/s (b).

Considering CF thread functionalization with Ppy functionalization, two different approaches were considered: the *in-situ* chemical polymerization of pyrrole (Ppy #1)(Figure 6.5, Supportive Information) and Ppy dispersion (Ppy #2). Then, the Ppy coated CF fibers were coated with CA and a twisted configuration was made with a CF as outer electrode.

The first approach showed a better coverage than the second one to the naked eye, and consequently, a better capacitive performance was obtained. Figure.3.14 shows the CV curves obtained for the Ppy#1(CF)/CF device. From them it can be seen a clear improvement in the device's maximum current (238 µA vs. 51 µA at 100 mV/s) and capacitance value which still shows high values even at high scan speeds, 306.9 mF/g at 40 mV/s and 80.4 mF/g at 1000 mV/s, which is approximately five times higher than the CF symmetrical SC. This enhancement is credited to the roughness of the Ppy layer created at the CF surface, which has more available surface area for ion adsorption [20][23].

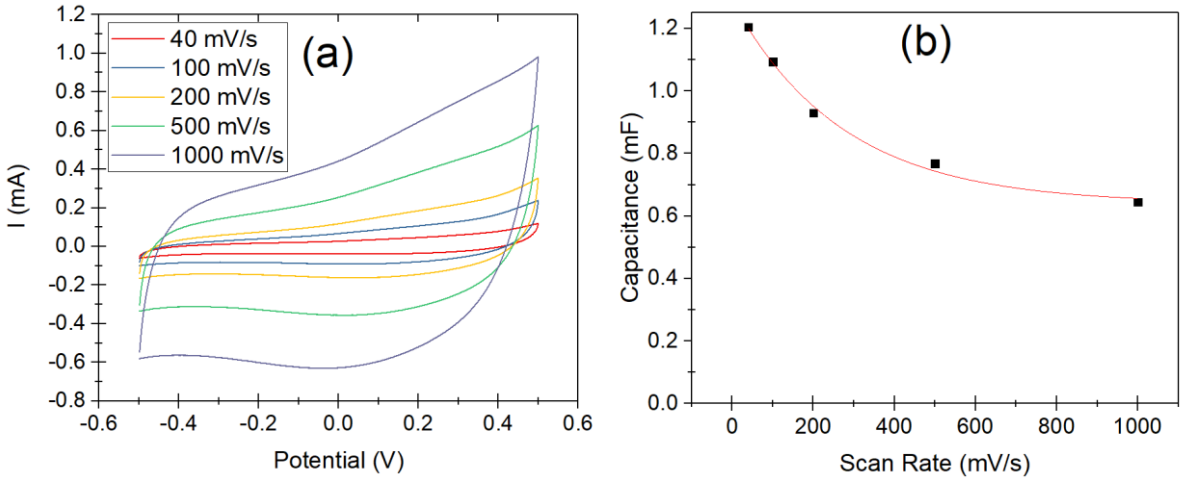

Fig. 3.14. Voltammograms of Ppy#1(CF)/CF. Cycling with different scan rates (a) and the calculated capacitance for each scan rate (b).

Considering the second approach (Ppy#2(CF)/CF), their voltammograms can be observed in Figure 3.15 (using the same electrode setup). In Figure 3.15 (a) a certain current improvement can be seen for high scan rates (299 µA vs. 154 µA at 1000 mV/s) , while at lower scan rates the device shows much similarity to the CF symmetrical SC (51 µA vs. 51 µA at 100 mV/s). This increase in maximum current can be possibly explained by the roughness of the Ppy#2 layer that allows more ion adsorption at high scan rates. A more typical square shaped curve is also observed which indicates lower resistance values (electrolyte and electrode). The calculated specific capacitance of the Ppy#2(CF)/CF device is 57.2 mF/g at 40 mV/s and 33.0 mF/g at 1000 mV/s which is similar to the one obtained for the CF electrode at low scan rates. Although, at high scan rates this device displays a better performance, resulting in a two times higher capacitance value possibly due to lower parasitic resistances. The studies on this sample were not continued due to weaker performance when compared with the Ppy #1(CF)/CF sample.

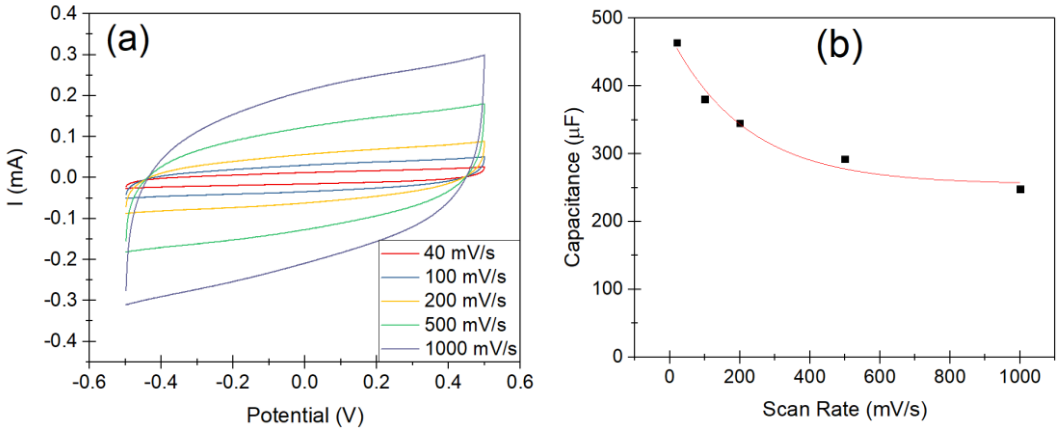

Fig. 3.15. Voltammograms of Ppy#2(CF)/CF. Cycling with different scan rates (a) and the calculated capacitance for each scan rate (b).

To compare the devices performance, the CV curve and specific capacitance at 100 mV/s obtained for each device is depicted in Figure 3.16 (a). All electrodes vary in size and weight; therefore, they were weighted before assembled to enable the calculation of their specific capacitance and obtain a more trustworthy comparison.

The CV curves obtained for Ppy#2(CF)/CF device and the ZnO:PVDF(CF)/CF one are similar to the symmetrical SC while the Ppy#1(CF)/CF shows a better performance. However, the specific capacitance determined for the ZnO:PVDF(CF)/CF sample is twice higher than the ones obtained for CF/CF SC at all rates (88 mF/g vs. 43 mF/g at 100 mV/s)(Figure 3.16 (b)). This enhancement can probably be improved with an optimized ZnO:PVDF ink to perform a more uniform coating on the CF surface. It is worth to mention that even though the Ppy#2(CF)/CF device didn't show much improvement on the specific capacitance at low scan rates. However, it can maintain its low capacitance at high scan rates. It is clear that the Ppy#1(CF)/CF sample shows the best performance (172 mF/g at 100 mV/s), therefore it was selected to carry on the study.

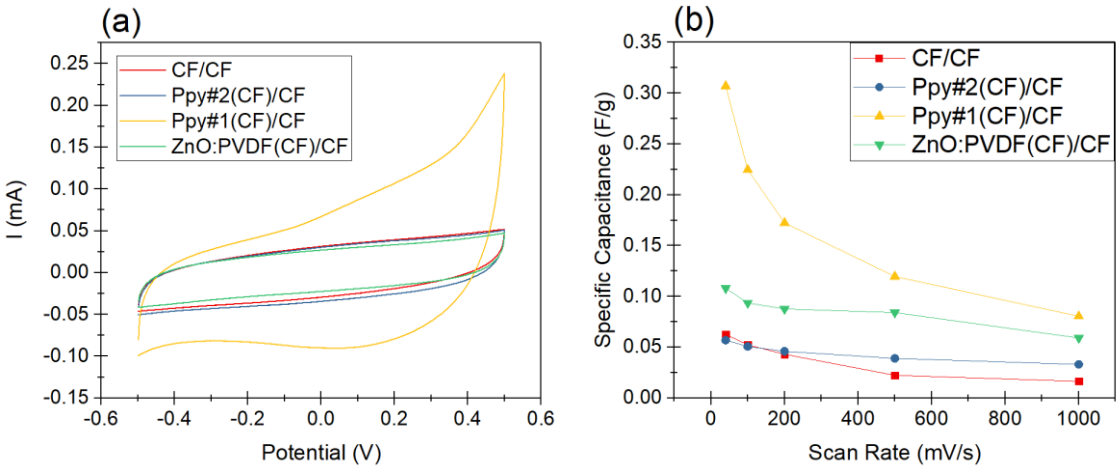

Fig. 3.16. Voltammograms of the previous SCs at 100 mV/s (a), and each sample specific capacitance at increasing scan rates (b).

3.2.1. Ppy#1(CF)/CF supercapacitor

Galvanostatic charge/discharge cycles were applied to the best sample (Ppy#1(CF)/CF) to complement the CV results and test its stability, the 34 cycles were fulfilled with a constant current of 7.7 mA/g and their calculated specific capacitance are shown in Figure 3.17 (b).

In Figure 3.17 (a) the 13th cycle is shown. From it, it's noticeable that the cycles are stranded between -504 and 322 mV (ΔV = 826 mV), which is not exactly the same interval used in the CV. However, the obtained specific capacitance values (approximately 468 mF/g) seem to be reasonable, when compared with the CV curves results and considering that these charge/discharge cycles have approximately a rate of 10 mV/s. Using equation 3 and 4, the energy and power density were calculated. From the specific capacitance, 468 mF/g, it was obtained an energy density of 159.65 mWh kg^{-1} and a power density of 11.49 W kg^{-1}, which are very low when compared with other devices [1][27][23].

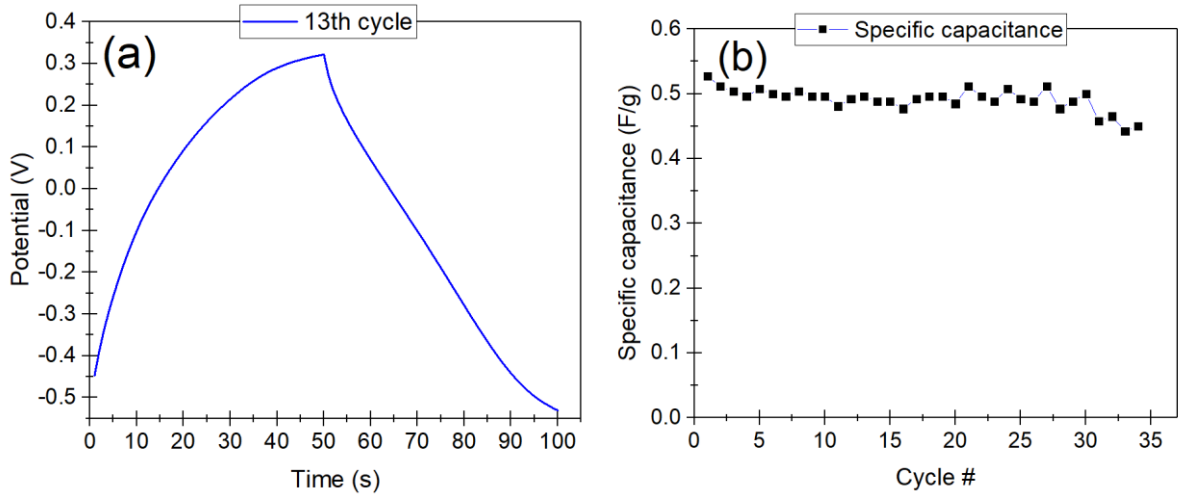

Fig. 3.17. CD plots of the Ppy#2(CF)/CF at 7.7 mA/g. Showing the 13th cycle (a) and the specific capacitance of 34 cycles (b).

The same sample was then submitted to 100 CV cycles at 100 mV/s to understand their electrochemical stability, the results can be found on Figure 3.18. From the shown cycles it's perceivable that all the curves are overlaid which translates in great cycling stability, with no significant capacitance lost.

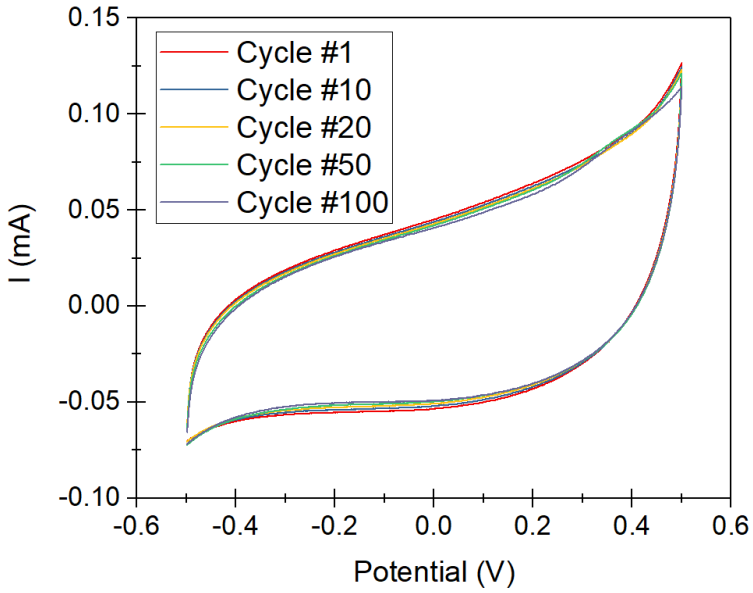

Fig. 3.18. Cyclic voltammetry of the previous samples for 100 cycles at 100 mV/s.

3.2.1.1. Electrochemical impedance spectroscopy analysis

For a better understanding of the capacitive behavior of the Ppy#1(CF)/CF device, electrochemical impedance spectroscopy (EIS) was employed on both, Ppy#1(CF)/CF device and the CF symmetrical SC from 1 MHz to 10 mHz. From the resulting plots (Figures 3.19, 3.20 and 3.21), it was possible to simulate an equivalent circuit model, calculate the equivalent series resistance and verify the device's capacitive behavior with incrementing frequency.

In Figure 3.19 it is shown that there is a phase change at low frequencies in both cases, indicating a capacitive behavior that quickly diminishes with increasing frequency. The best capacitive behavior is found at frequencies lower than 10 Hz which is characterized by a constant phase capacitor parallel to a charge transfer resistance (Figure 3.19 and 3.20) [28]. At these frequencies it can be seen a good capacitive stability in both samples. The phase peak change is very similar in both cases, -54º in CF/CF and -55º in Ppy#1(CF)/CF. Since the phase peak does not fall to -90º, it was assumed that these devices possess leakage and/or diffusion effects that jeopardize their ideal capacitor behavior, most likely a charge transfer impedance [29]. This effect can be overcome with a less resistive separator/electrolyte and an optimized processing, which can result in a more homogeneous and consistent Ppy layer. At higher frequencies (above 10 Hz) the phase angle is 45º and it decreases sharply to 0º as well as the capacitance, which is a common event on porous electrodes due to the inability of access from the electrolyte ions to the inner pores of the electrode [29]. The maximum specific capacitance, that can be found at approximately 0.1 Hz, is 196 mF/g for the Ppy#1(CF)/CF and 68 mF/g for the CF/CF, which seem to be in agreement with the previous results (Figure 3.16).

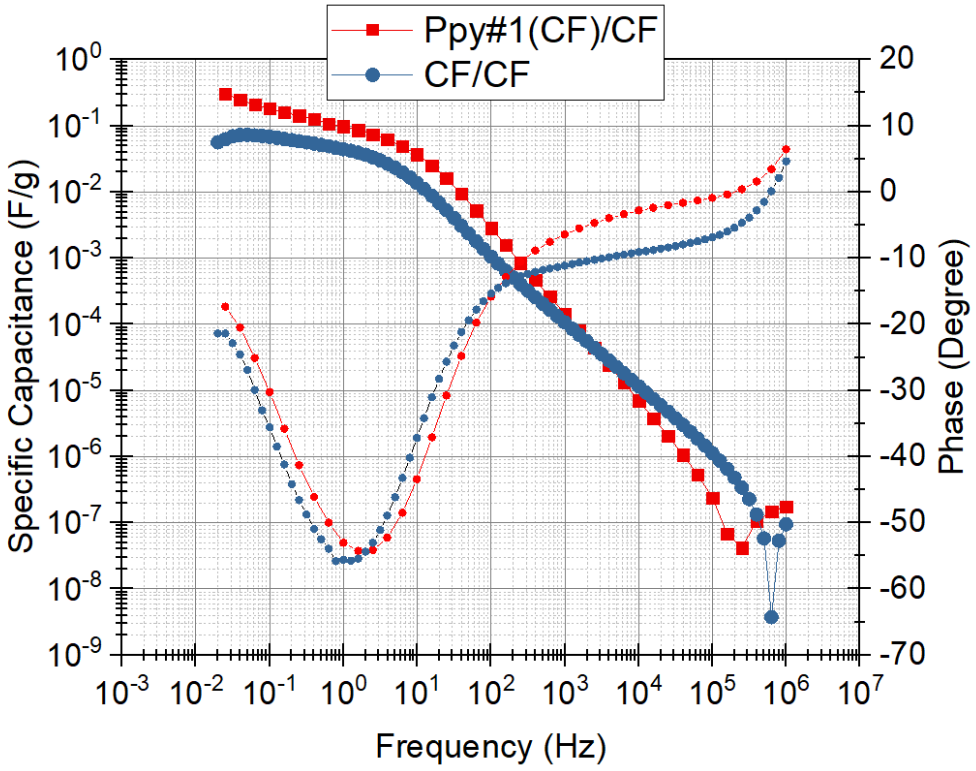

Fig. 3.19. EIS, bode plot from CF/CF in blue and from Ppy#1(CF)/CF in red at 100 mV/s. The impedance was replaced with the specific capacitance and it's represented by the squares. While the phase is represented by the small circles.

The Nyquist plot obtained from the EIS analysis of Ppy#1(CF)/CF and the CF/CF SC can be found on Figure 3.20 and 3.21 with an equivalent circuit usually used for modelling diffusion processes. The black line shows the fitting made with the model. In both cases the model suggests a resistive behavior on the surface and a more complex capacitive behavior in the sample's bulk. The models are made with an uncompensated solution resistance (Ru), a charge transfer resistance (Rct), a constant phase capacitor (CPE) which simulate the behavior of a double layer capacitance, and in the Ppy#1(CF)/CF a Warburg impedance (Wd) that model the diffusion resistance process and result in a better fitting for experimental data [30]. The interception of the curve with the real impedance axis indicates the equivalent series resistance (ESR) which includes the intrinsic electrodes (CF and Ppy), electrolytes and contact resistance of the SC, which for the CF/CF sample is 55.13 Ω and for the Ppy#1(CF)/CF device is 36.99 Ω [31][29]. In the high frequency region (> 1kHz), both devices offer no internal resistance thus losing the ability to store charge. They showed a limited charge diffusion process around 1 kHz, represented by the semi-circle, followed by a more horizontal line which may be due to the electrolyte's diffusion impedance or, for the Ppy(CF)/CF, a pseudocapacitive behavior inputted by the Ppy coverage [32]. Both samples show high impedance, however, the last one maintains its real impedance lower than 3 kΩ while the CF go as high as 20 kΩ. Furthermore, the semi-circle is much well defined for the Ppy#1(CF)/CF SC than for the CF/CF one, indicating a more capacitive behavior thus a better electrochemical performance.

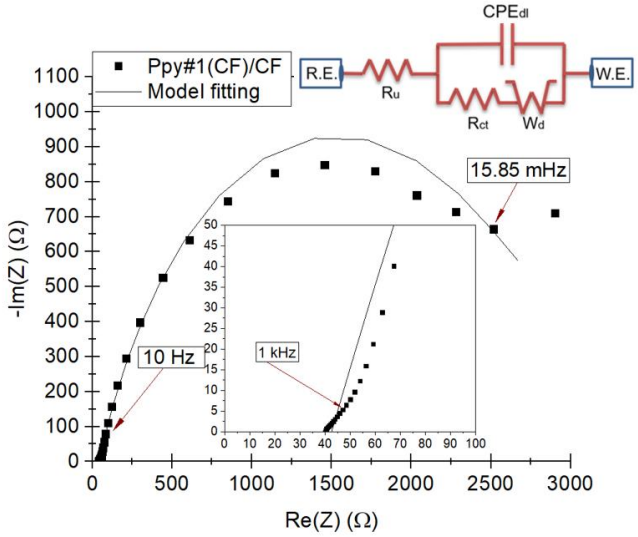

Fig. 3.20. EIS, Nyquist plot from Ppy#1(CF)/CF accompanying the previous bode plot. In it there is the zoomed area from the high frequency region. The present fitting is provided by the model on top.

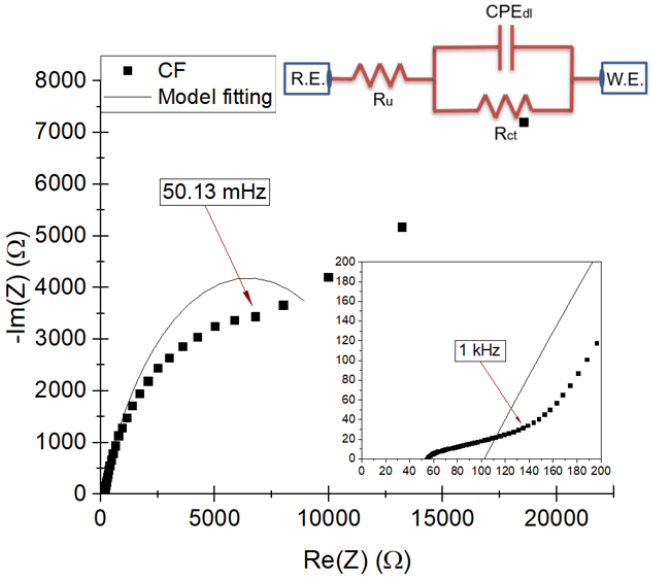

Fig. 3.21. EIS, Nyquist plot from CF/CF accompanying the previous bode plot. In it there is the zoomed area from the high frequency region. The present fitting is provided by the model on top.

Although the improvement was somewhat successful, their specific capacitance values are very low when compared to the literature (Table 3.2) [1][18][19]. It was suspected that the SBF jeopardized the good performance of the device, therefore a KOH solution of 0.1 M was used to replace the SBF as electrolyte for a better comparison with the literature.

A symmetrical Ppy#1(CF) device was employed for the KOH experiment, the results are shown in Figure 3.22. It is worth to mention that Figure 3.22 (b) does not go beyond 100 mV/s for the CV study, therefore comparison with other results must be made cautioned. By looking at these CV curves it's noticeable that the cycles are far from ideal and show a considerable series and parallel resistance.

However, the maximum current of this device (1.35 mA at 100 mV/s) is greater than the one using SBF (0.24 mA at 100 mV/s), which indicates a higher accumulated charge. From the specific capacitance plot it can be confirmed the dramatic improvement. Using only a 0.1M KOH solution as electrolyte the specific capacitance from the device seems to improve, specifically from 0.172 F/g, to 3.60 F/g at 100 mV/s. This improvement demonstrates that SBF is energetically weaker when compared with KOH (0.1M), for electrolyte use in wearable energy storage applications.

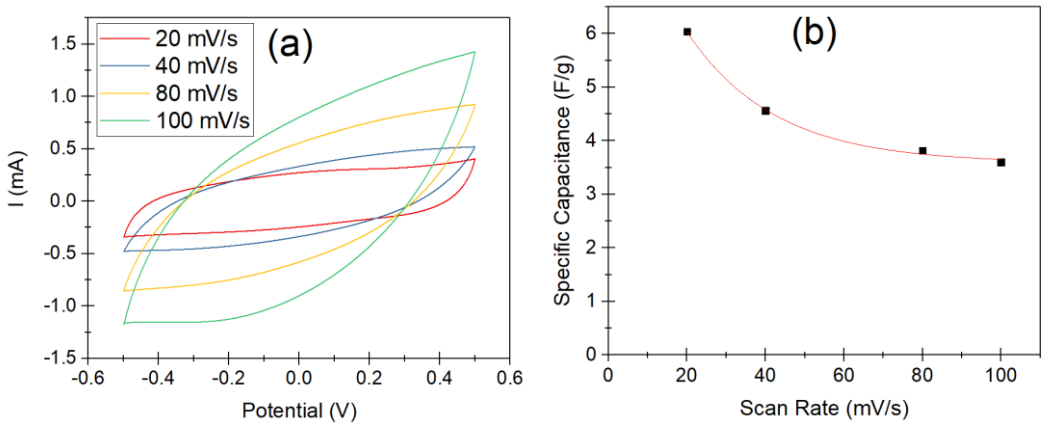

Fig. 3.22. Voltammograms of a Ppy#1(CF) symmetrical SC with KOH (0.1M) as electrolyte. Cycling with different scan rates (a), and the calculated specific capacitance of each scan rate (b).

Ppy#1(CF)/CF soaked in SBF and in KOH (0.1M), specific capacitance was later compared with the works reported in the literature (Table 3.2). From Table 3.2 it's noticeable that the PPy#1(CF)/CF shows inferior capacitance. Therefore, a better improvement can be made using a higher concentration KOH solution, or a gel electrolyte, and/or a more optimized device processing (separator thickness and active material thickness).

Table. 3.2. Comparison of the specific capacitance values obtained in this work with the ones reported in literature.

Supercapacitor	**Electrolyte**	**Specific Capacitance (F/g)**	**Configuration**
Ppy#1(CF)/CF	SBF	0.17 – 0.31 F/g (100 – 40 mV/s)	Twisted
Ppy#1(CF)/CF	KOH (0.1M)	3.6 – 6 (100 – 20 mV/s)	Twisted
Graphene:Ppy symmetrical [19]	H_2SO_4:PVA (gel)	72 F/g (10 mV/s)	Twisted (Parallel)
Graphite:ZnO(Cu) symmetrical [18]	NaCl(1M):PVP (gel)	9 – 27 F/g (100 – 10 mV/s)	Twisted (Parallel)

4. Conclusion and Future Perspectives

Here various electrode materials were tested to serve a wearable supercapacitor for wearable applications, with a CA separator soaked in SBF to simulate our body sweat. However, most of these materials showed mechanical weaknesses that were not adequate for wearable applications, such as the carbon ink, the GE:PVDF wire and the ZnO:PVDF ink. While others demonstrated high electrochemical cyclic instability triggered by the electrode's breakdown, these include the Al wire, the carbon ink and the thermally evaporated Cu shown by photographs and SEM results on Figure 3.2 – 3.5. In the Al wire case, the electrode suffered from the pitting phenomenon where chlorine ions erode the passive oxide layer and disintegrate the wire [25]. Therefore, CF were the prime choice for electrode material. Having great thread-like flexibility and optimal electrical conductivity, the focus was on them. However, with the first experiment made (Figure 3.12) it was verified that the CF/CF SC displayed a low specific capacitance of 43 mF/g at 100 mV/s. Coaxial (core-shell) structures were abandoned from here on due to the hardness of making a layer material that can accompany the inner electrode's flexibility.

Electrode functionalization with pseudocapacitive materials, namely ZnO:PVDF and Ppy, were made to increase the CF electrochemical properties. The prior was made using PVDF and ZnO in DMF, followed by the covering of the CF with this solution. The result showed a white rigid wire that was wrapped around a CA covered CF, making a twisted structure. This device showed an improvement in cycling stability and in specific capacitance (88 mF/g at 100 mV/s) when compared to the original CF symmetrical device. However, the lack of flexibility made this device unfit for wearable applications.

In order to improve the electrochemical properties of the CF without losing much flexibility, Ppy was employed. Two different covering methods were used and compared, the *in-situ* polymerization (Ppy#1(CF)/CF) and another where Ppy was dissolved in acetone and deposited on the CF surface (Ppy#2(CF)/CF). The latter results showed very little improvement with the same specific capacitance as the CF at scan rates lower than 100 mV/s (51 mF/g at 100 mV/s). However, at higher rates the Ppy#2(CF)/CF SC shows better stability with 33 mF/g at 1000 mV/s, which the CF/CF one only demonstrated 16.4 mF/g. In summary, Ppy#1(CF)/CF show better performances. Revealing 225 mF/g at 100 mV/s its specific capacitance is approximately 5 times higher than the CF symmetrical one, even at high scan rates. Since Ppy#1(CF)/CF SC showed the best results by far, it was submitted to CV cycling, CD and EIS to understand better its electrochemical behaviour.

The CV cycling did not show any significant difference from the 1st to the 100th curve therefore this SC shows optimal cycling stability as expected [1][2][27]. However, from the CD capacitance curve it's noticeable a small diminish on the specific capacitance possibly due to the SBF's drying. From these CD results it was possible to calculate the device's specific capacitance and consequently its energy and power density. The calculated specific capacitance (468 mF/g) seems to be in agreement with the CV results if considering a scan rate of 10 mV/s. Hence the resulting energy and power density are

159.65 mWh kg^{-1} and 11.49 W kg^{-1} respectively, which is low when compared with the literature [19][18] but can be used to power small health monitoring devices. From the EIS results it was concluded that the CF symmetrical SC have an ESR of 55.13 Ω and the Ppy #1 SC has 36.99 Ω. Additionally it was verified a very high internal resistance in both cases, especially in the CF which at 50 mHz shows 6.8 kΩ while the Ppy #1 sample shows 1.7 kΩ at the same frequency. This result indicates that the electrolyte ions have difficulty diffusing due to the Ppy layer or the CA in use are not optimized in thickness nor in porosity. However, a definitive improvement on the CF electrode by covering it with a Ppy layer that enables pseudocapacitance was successfully executed. Still, the results were not the expected due to very small capacitance values when compared with the literature [1][27][20][23]. Thus, SBF was replaced with 0.1 M of KOH to comprehend if the weak capacitance is due to the electrolyte. There was a clear improvement of the device's specific capacitance (0.23 F/g to 3.60 F/g at 100 mV/s) which indicates that SBF is not the most suitable electrolyte. However, it is possible to adapt this device for biomedical monitoring applications, where a biosensor uses the energy and/or information stored in this SC from the users sweat.

The Ppy#1(CF)/CF SC can be further optimized for different applications, using a stronger electrolyte or even a polyelectrolyte; it can be achieved much higher specific capacitance and consequently, energy and power densities. Regarding the use of this device in wearable electronics, it is also fundamental to evaluate the device mechanical properties under different bending ratios and to study the specific capacitance retention under several bending cycles.

5. References:

[1] H. Sun, Y. Zhang, J. Zhang, X. Sun, and H. Peng, “Energy harvesting and storage in 1D devices,” *Nat. Rev. Mater.*, vol. 2, no. 6, p. 17023, Apr. 2017.

[2] L. Dong *et al.*, “Flexible electrodes and supercapacitors for wearable energy storage: a review by category,” *J. Mater. Chem. A*, vol. 4, no. 13, pp. 4659–4685, 2016.

[3] F. Yi, H. Ren, J. Shan, X. Sun, D. Wei, and Z. Liu, “Wearable energy sources based on 2D materials,” *Chem. Soc. Rev.*, vol. 47, no. 9, pp. 3152–3188, May 2018.

[4] K. Jost, G. Dion, and Y. Gogotsi, “Textile energy storage in perspective,” *J. Mater. Chem. A*, vol. 2, no. 28, p. 10776, 2017.

[5] A. E. Ostfeld, A. M. Gaikwad, Y. Khan, and A. C. Arias, “High-performance flexible energy storage and harvesting system for wearable electronics,” *Sci. Rep.*, vol. 6, no. 1, p. 26122, Sep. 2016.

[6] Y. Wang *et al.*, “3D-Printed All-Fiber Li-Ion Battery toward Wearable Energy Storage,” *Adv. Funct. Mater.*, vol. 27, no. 43, p. 1703140, 2017.

[7] A. Sumboja, J. Liu, W. G. Zheng, Y. Zong, H. Zhang, and Z. Liu, “Electrochemical energy storage devices for wearable technology: a rationale for materials selection and cell design,” *Chem. Soc. Rev.*, vol. 47, no. 15, pp. 5919–5945, 2018.

[8] W. Liu *et al.*, “3D Porous Sponge-Inspired Electrode for Stretchable Lithium-Ion Batteries,” *Adv. Mater.*, vol. 28, no. 18, pp. 3578–3583, May 2016.

[9] A. M. Zamarayeva *et al.*, “Flexible and stretchable power sources for wearable electronics,” *Sci. Adv.*, vol. 3, pp. 1602051–1602061, 2017.

[10] Z. Liu, G. Li, T. Cui, A. Borodin, C. Kuhl, and F. Endres, “A battery-supercapacitor hybrid device composed of metallic zinc, a biodegradable ionic liquid electrolyte and graphite,” *J. Solid State Electrochem.*, vol. 22, no. 1, pp. 91–101, 2018.

[11] M.-C. Lin *et al.*, “An ultrafast rechargeable aluminium-ion battery,” *Nature*, vol. 520, no. 1, pp. 324–328, 2015.

[12] J. Kang, J. Wen, H. S. Jayaram, A. Yu, and X. Wang, “Development of an equivalent circuit model for electrochemicaldouble layer capacitors (EDLCs) with distinct electrolytes,” *Electrochim. Acta*, vol. 115, pp. 587–598, 2014.

[13] G. Z. Chen, “Understanding supercapacitors based on nano-hybrid materials with interfacial conjugation,” *Prog. Nat. Sci. Mater. Int.*, vol. 23, no. 3, pp. 245–255, 2013.

[14] A. G. Pandolfo and A. F. Hollenkamp, “Carbon properties and their role in supercapacitors,” *J. Power Sources*, vol. 157, no. 1, pp. 11–27, 2006.

[15] T. Qin *et al.*, “Flexible and Wearable All-Solid-State Supercapacitors with Ultrahigh Energy Density Based on a Carbon Fiber Fabric Electrode,” *Adv. Energy Mater.*, vol. 7, p. 1700409, Jul. 2017.

[16] V. Thong Le *et al.*, “Coaxial Fiber Supercapacitor Using All-Carbon Material Electrodes,” *ACS Nano*, vol. 7, no. 7, pp. 5940–5947, 2013.

[17] J. G. Wang, Y. Yang, Z. H. Huang, and F. Kang, “Coaxial carbon nanofibers/MnO2nanocomposites as freestanding electrodes for high-performance electrochemical capacitors,” *Electrochim. Acta*, vol. 56, no. 25, pp. 9240–9247, 2011.

[18] A. Rafique, S. Bianco, M. Fontana, C. F. Pirri, and A. Lamberti, “Flexible wire-based electrodes exploiting carbon/ZnO nanocomposite for wearable supercapacitors,” *Ionics (Kiel).*, vol. 23, no. 7, pp. 1839–1847, 2017.

[19] Y. Hu *et al.*, “Spinning fabrication of graphene/polypyrrole composite fibers for all-solid-state, flexible fibriform supercapacitors Spinning fabrication of graphene/polypyrrole composite fibers for all-solid-state, flexible fibriform supercapacitors †,” *J. Mater. Chem. A*, vol. 2, no. 31, pp. 12355–12360, 2014.

[20] Y. Huang *et al.*, “Nanostructured Polypyrrole as a flexible electrode material of supercapacitor,” *Nano Energy*, vol. 22, pp. 422–438, 2016.

[21] L. Hu *et al.*, “Symmetrical MnO 2 - Carbon Nanotube - Textile Nanostructures for Wearable Pseudocapacitors with High Mass Loading,” *ACS Nano*, vol. 5, no. 11, pp. 8904–8913, 2011.

[22] X. Li *et al.*, “High-Performance Polypyrrole/Graphene/SnCl $_2$ Modified Polyester Textile Electrodes and Yarn Electrodes for Wearable Energy Storage,” *Adv. Funct. Mater.*, vol. 28, no. 22, p. 1800064, May 2018.

[23] M. Raicopol, A. Pruna, and L. Pilan, “Supercapacitance of Single-Walled Carbon Nanotubes-Polypyrrole Composites,” *J. Chem.*, vol. 2013, pp. 1–7, Aug. 2013.

[24] A. C. Baptista *et al.*, “Cellulose-based electrospun fibers functionalized with polypyrrole and polyaniline for fully organic batteries,” *J. Mater. Chem. A*, vol. 6, no. 1, pp. 256–265, Dec. 2018.

[25] C. M. A. Brett, I. A. R. Gomes, and J. P. S. Martins, “The electrochemical behaviour and corrosion of aluminium in chloride media. The effect of inhibitor anions,” *Corros. Sci.*, vol. 36, no. 6, pp. 915–925, 1994.

[26] S. Jalota, S. B. Bhaduri, and A. C. Tas, “Using a synthetic body fluid (SBF) solution of 27 mM HCO3− to make bone substitutes more osteointegrative,” *Mater. Sci. Eng. C*, vol. 28, no. 1, pp. 129–140, Jan. 2008.

[27] Q. Liu *et al.*, “A Flexible and Knittable Fiber Supercapacitor for Wearable Energy Storage with High Energy Density and Mechanical Robustness,” *J. Electrochem. Soc.*, vol. 165, no. 7, pp.

1515–1522, 2018.

[28] S. S. Shinde, G. S. Gund, V. S. Kumbhar, B. H. Patil, and C. D. Lokhande, “Novel chemical synthesis of polypyrrole thin film electrodes for supercapacitor application,” *Eur. Polym. J.*, vol. 49, no. 11, pp. 3734–3739, Nov. 2013.

[29] H. Feng *et al.*, “Three-dimensional honeycomb-like hierarchically structured carbon for high-performance supercapacitors derived from high-ash-content sewage sludge,” *J. Mater. Chem. A*, vol. 3, no. 29, pp. 15225–15234, 2015.

[30] “Basics of EIS: Electrochemical Research-Impedance.” [Online]. Available: https://www.gamry.com/application-notes/EIS/basics-of-electrochemical-impedance-spectroscopy/.

[31] V. Rajeswari, R. Jayavel, and A. C. Dhanemozhi, “Synthesis And Characterization Of Graphene-Zinc Oxide Nanocomposite Electrode Material For Supercapacitor Applications,” *Mater. Today Proc.*, vol. 4, no. 2, pp. 645–652, 2017.

[32] K. V. Sankar and R. K. Selvan, “The preparation of MnFe2O4 decorated flexible graphene wrapped with PANI and its electrochemical performances for hybrid supercapacitors,” *RSC Adv.*, vol. 4, no. 34, p. 17555, 2014.

6. Supporting Information

6.1. Electrospinning setup:

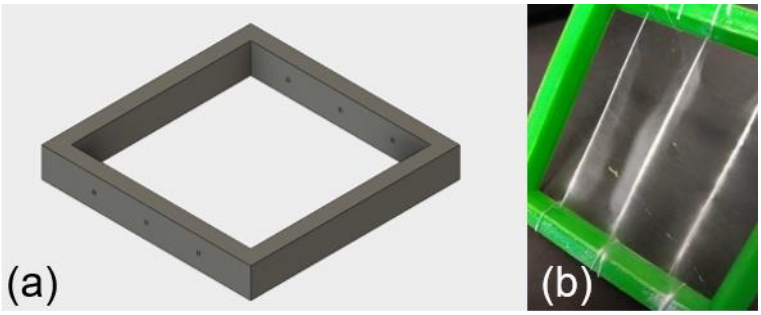

Fig. 6.1. The software design of the frame on the left and the real 6 x 6 cm frame pos-deposition on the right.

Fig. 6.2. Photo of the electrospinning layout with 3 Al wires as collector.

6.2. Samples photos and SBF composition:

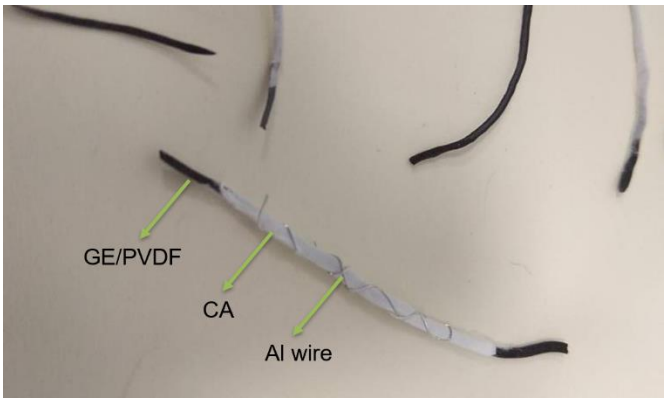

Fig. 6.3. Photo from GE/PVDF wires. With some covered in CA, and one of them as a built device with Al as outer electrode.

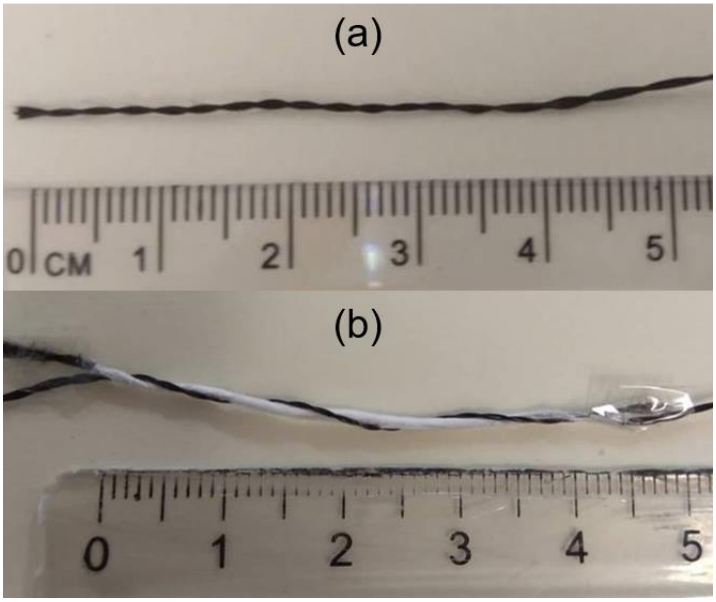

Fig. 6.4. Photos of the CF (a) and the built CF symmetrical SC (b)

Table. 6.1. SBF composition, adapted from [26].

Order:	**Reagent**	**Quantity (g/l)**
1	NaCl	6.547
2	$NaHCO_3$	2.268
3	KCl	0.373
4	$Na_2HPO_4.2H_2O$	0.178
5	$MgCl_2.6H_2O$	0.305
6	1M HCl	15 mL
7	$CaCl_2.2H_2O$	0.368
8	Na_2SO_4	0.071
9	$(CH_2OH)_3CNH_2$	6.057
10	1M HCl	Add until pH = 7.4 at 37 ºC

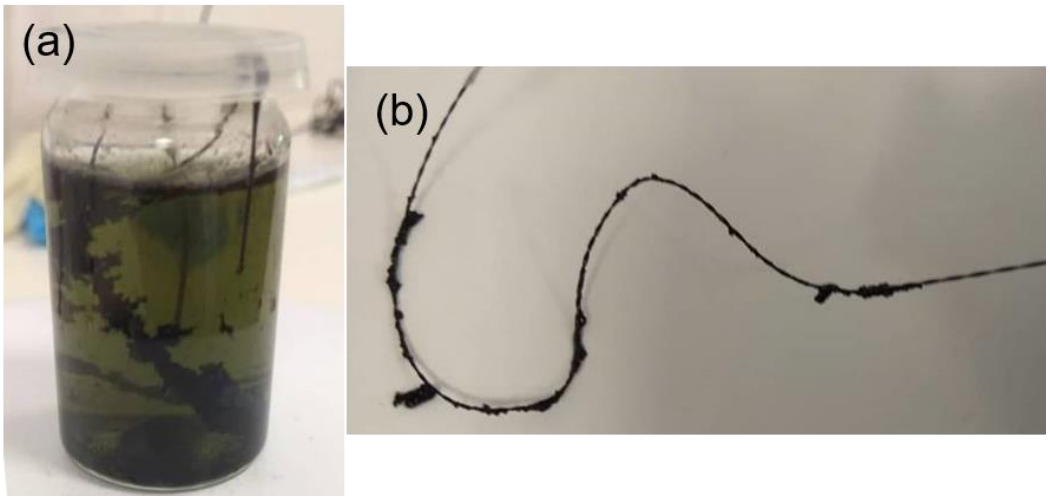

Fig. 6.5. Photos of the *in-situ* Ppy polymerization (a) and the resulting fiber pre-washed (b).

6.3. Electrochemical testing setup:

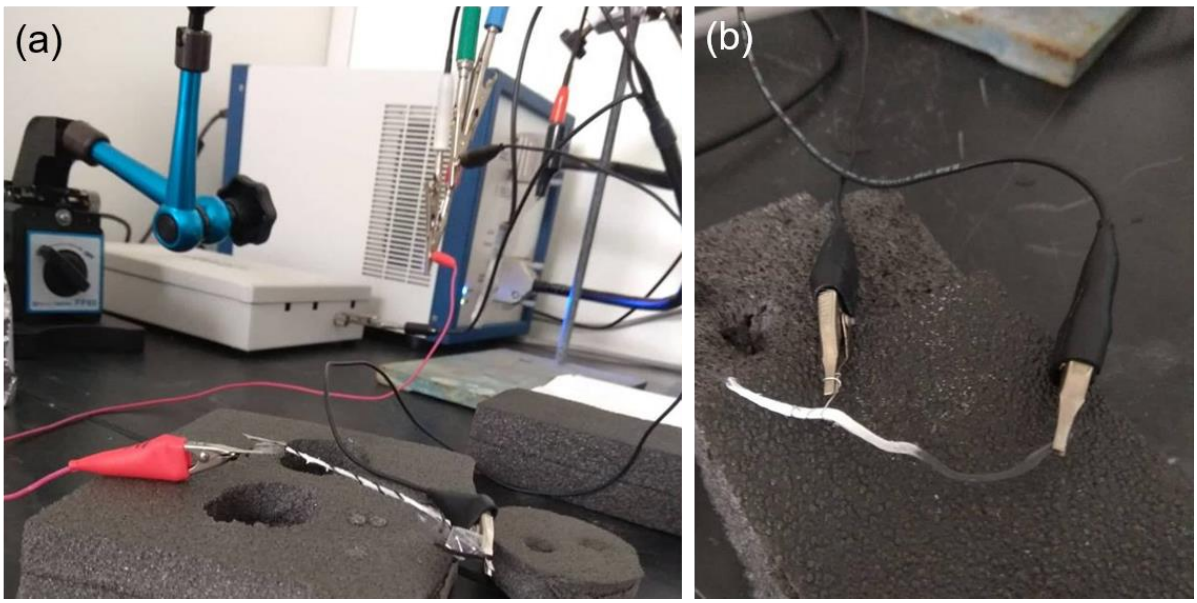

Fig. 6.6. Photos of the electrochemical, two-electrode, setup. A CF symmetrical SC (a) and a GE/PVDF with Al SC (b) being measured.

6.4. Electrospun CA layer thickness:

Electrospun CA layers were used as separator for the various built devices. Different deposition times (15 minutes/side, 30 minutes/side or 1 hour/side) were tested using 3 CF to collect the electrospun fibers on the previously discussed frame. The resulting CA layer thickness were measured using a micrometer. To achieve this, the samples were place between two small glasses with known thickness according to Figure 6.7. These were then subtracted from the result as well as the CF thickness, the outcome was divided by 2 to achieve the CA layer thickness shown on Table 6.1. Afterwards, Al wires were used to wrap around the CA covered CF and the subsequent energy storage device was submitted to CV testing. Where the Al wire was connected to the reference/counter electrode.

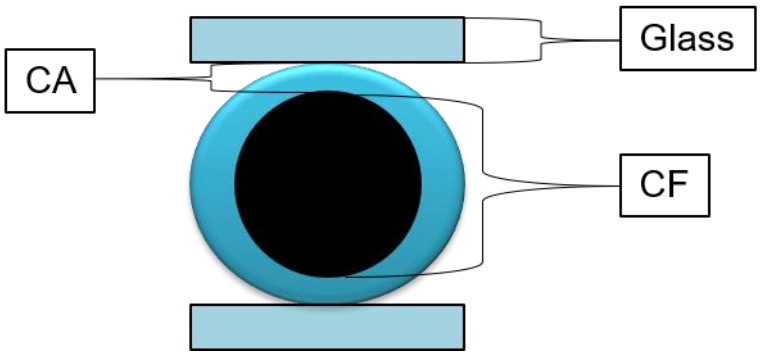

Fig. 6.7. Schematic of the cross section from the resulting fiber. Highlighting the thicknesses.

Table. 6.2. CA layer deposition time and respective measured thicknesses.

Deposition Time:	**15 minutes/side**	**30 minutes/side**	**60 minutes/side**
CA layer thickness:	157 +/- 30.5 µm	207.5 +/- 10.5 µm	302.5 +/- 17 µm

All samples showed non-homogeneous thickness along the fiber length. On the 15 minutes/side device hardship was found trying to prevent short-circuit from the inner to the outer electrode. While on the 60 minutes/side there was difficulties absorbing the electrolyte, probably due to the high CA fiber density. Therefore, the 30 minutes/side deposition time was chosen for the other devices.